Water Resources Research

RESEARCH ARTICLE
10.1029/2023WR035817

Special Section:
Hydrogeodesy: Understanding changes in water resources using space geodetic observations

Reinterpreting Global GRACE Trends Based on Century-Long GRACE-REC Data

Yulong Zhong[1,2], Baoming Tian[1], Bramha Dutt Vishwakarma[3,4], Wei Feng[5], Yunlong Wu[1], Hongbing Bai[1,5], and Min Zhong[5]

[1]School of Geography and Information Engineering, China University of Geosciences (Wuhan), Wuhan, China, [2]Artificial Intelligence School, Wuchang University of Technology, Wuhan, China, [3]Interdisciplinary Centre for Water Research, Indian Institute of Science, Bangalore, India, [4]Centre for Earth Science, Indian Institute of Science, Bangalore, India, [5]School of Geospatial Engineering and Science, Sun Yat-Sen University, Zhuhai, China

Abstract Assessing changes in freshwater availability accurately is crucial for societal development. Previous studies have examined long-term variations in basin-scale terrestrial water storage (TWS) using Gravity Recovery and Climate Experiment (GRACE) mission data. However, different basins exhibit distinct spatial and temporal TWS variation patterns. To better interpret the TWS trends in each basin during the GRACE era (2003–2016), this study proposes a novel criterion based on a century-long GRACE-REC data set. This criterion assesses the trends in GRACE TWS ($Trend_G$), precipitation-induced trends ($Trend_{PI}$), and non-precipitation-induced trends ($Trend_{NPI}$) over the GRACE period. By calculating upper and lower bound values for long-term climate-driven TWS trends using GRACE-REC data, an indicator is provided to evaluate the range of TWS trend variations in a basin under natural conditions. Results reveal that among the 266 global basins analyzed in this study, the trends ($Trend_G$, $Trend_{PI}$, or $Trend_{NPI}$) in 115 basins exceed the maximum or minimum water storage trends associated with natural climate variability. This includes 20 large basins, 34 medium basins, and 61 small basins, indicating significant TWS changes during the GRACE period. Furthermore, we analyze the driving mechanisms of TWS trends in the 20 large basins using multi-source data. The mechanisms identified through this method align well with both our analysis and previous studies, confirming the reliability of this approach for assessing TWS trends.

Plain Language Summary Understanding changes in freshwater availability is crucial for the development of human societies. This study focuses on assessing long-term changes in basin-scale terrestrial water storage (TWS) using data from the Gravity Recovery and Climate Experiment (GRACE) mission. The objective of this research was to develop a new criterion to assess TWS trends in different basins during the GRACE era. We calculated the upper and lower bound values of long-term climate-driven TWS trends for a given length of time, analyzed the trends induced by precipitation and non-precipitation factors, and examined the driving mechanisms behind TWS trends in selected basins. Among the 266 global basins analyzed, 115 basins showed TWS trends that exceeded the trend bounds under natural climate variability. This indicates significant changes in TWS during the GRACE period. Our analysis of driving mechanisms aligned well with previous studies, providing confidence in the reliability of our approach. Our study reveals significant changes in TWS in numerous basins worldwide, highlighting the importance of monitoring and managing water resources effectively.

Key Points:

- A novel criterion is proposed to interpret trends in Gravity Recovery and Climate Experiment (GRACE), precipitation-induced, and non-precipitation-induced water storage
- The upper and lower bounds of long-term climate-driven terrestrial water storage (TWS) trends are estimated based on one century-long GRACE-REC data
- Significant non-precipitation effects contribute to GRACE trends below the lower bounds of climate-driven TWS trends in global basins

Supporting Information:

Supporting Information may be found in the online version of this article.

Correspondence to:

W. Feng and Y. Wu,
fengwei@sysu.edu.cn;
wuyunlong@cug.edu.cn

Citation:

Zhong, Y., Tian, B., Vishwakarma, B. D., Feng, W., Wu, Y., Bai, H., & Zhong, M. (2023). Reinterpreting global GRACE trends based on century-long GRACE-REC data. *Water Resources Research*, *59*, e2023WR035817. https://doi.org/10.1029/2023WR035817

Received 14 JUL 2023
Accepted 23 NOV 2023

Author Contributions:

Conceptualization: Yulong Zhong, Baoming Tian, Wei Feng
Formal analysis: Yulong Zhong, Wei Feng, Yunlong Wu

1. Introduction

Terrestrial water storage (TWS) encompasses various components of water near the Earth's surface, including groundwater, soil moisture, surface waters, and snow water equivalent (Humphrey et al., 2023; Tapley et al., 2019). Accurate assessment of TWS is essential for food security, human and ecosystem health, energy supply, and socioeconomic development (Huggins et al., 2022; Pokhrel et al., 2021; Shen et al., 2022). As the primary water source for humans, surface water supplies are becoming increasingly unpredictable with more droughts and floods (Kundzewicz et al., 2007; Rodell & Li, 2023; Tabari et al., 2021), which has led to a growing dependence on groundwater as a resilient water supply during droughts (Famiglietti, 2014; Scanlon et al., 2023; Taylor et al., 2013). Globally, over 2 billion people rely on groundwater as their primary source of freshwater (Gleeson et al., 2012). With precipitation and river hydrology undergoing significant changes (Syed et al., 2010), certain regions face an increasing threat to biodiversity (Vorosmarty et al., 2010), while approximately 4 billion

Funding acquisition: Yulong Zhong, Bramha Dutt Vishwakarma, Wei Feng, Yunlong Wu, Min Zhong
Investigation: Yulong Zhong, Baoming Tian
Methodology: Yulong Zhong, Baoming Tian, Bramha Dutt Vishwakarma, Hongbing Bai
Resources: Wei Feng, Yunlong Wu
Supervision: Yulong Zhong, Wei Feng, Yunlong Wu
Validation: Yulong Zhong, Baoming Tian, Bramha Dutt Vishwakarma
Visualization: Yulong Zhong, Baoming Tian
Writing – original draft: Yulong Zhong, Baoming Tian
Writing – review & editing: Yulong Zhong, Bramha Dutt Vishwakarma, Wei Feng, Yunlong Wu, Hongbing Bai, Min Zhong

people worldwide suffer from severe water deficits (Mekonnen & Hoekstra, 2016). The decline in aquifer water levels will only worsen throughout the 21st century due to the increasing food demand driven by global population growth (Turner et al., 2019). Therefore, it is crucial to track global or regional changes in TWS (TWSC).

However, monitoring global or regional TWSC has become challenging due to limited publicly shared in situ data from hydrological stations, primarily driven by political and economic pressures (J. Chen et al., 2016). Fortunately, satellite remote sensing and geodesy offer an excellent solution to this problem, providing a global perspective that transcends political boundaries (Famiglietti et al., 2015). In particular, the Gravity Recovery and Climate Experiment (GRACE) mission and its follow-on, GRACE-FO, have presented a new opportunity for water resource monitoring (Landerer et al., 2020; Tapley et al., 2004). Previous studies have demonstrated that GRACE detected TWS deficits in various regions, particularly those with intensive irrigated agriculture and high population densities, for example, the North China Plain (Feng et al., 2013; Huang et al., 2015; Long et al., 2023), northern India (Tiwari et al., 2009), the Middle East (Amiri et al., 2023; Joodaki et al., 2014), and California's Central Valley (P. W. Liu et al., 2022). GRACE has also been successful in monitoring drought-induced water storage depletion, as observed during the Central European droughts in 2018 and 2019 (Boergens et al., 2020), and the Yangtze River Basin drought in 2019 (Y. Ran et al., 2021). Furthermore, the shrinking of glaciers or ice sheets has been observed in regions such as the Gulf of Alaska coast (Luthcke et al., 2013), southeastern Tibetan Plateau (Li et al., 2022; Zhao et al., 2022), Patagonia (J. Chen et al., 2007; Tapley et al., 2019), and Greenland, and Antarctica (J. Ran et al., 2021; Velicogna et al., 2020). On the other hand, some regions have experienced an increase in TWS, including the northern Great Plains, Okavango River Basin, southeastern South America, eastern Australia (Rodell et al., 2018), and southeastern China (Mo et al., 2016). However, fewer studies have compared the different TWS trend values derived from GRACE across global basins (Scanlon et al., 2016).

The GRACE mission has been successfully applied to monitor phenomena such as glacier melting and ocean mass change, yielding promising results (Ramillien et al., 2008; Wouters et al., 2014). Typically, the TWS anomaly (TWSA) time series is decomposed into a seasonal term and a trend term calculated through various fitting methods. Several studies have utilized the magnitude of TWS trends to evaluate the severity of water deficits and rank areas based on water stress (Famiglietti, 2014; Richey et al., 2015). Recently, other studies have employed the percentage of trend variance relative to the total TWS variance or R^2 value (Rodell et al., 2018; Scanlon et al., 2022; Shamsudduha & Taylor, 2020), and the ratio of the trend to interannual variability from reconstructed TWS data, or the GRACE data (Scanlon et al., 2022; Vishwakarma et al., 2021). Inspired by these studies and considering two challenges faced in previous trend assessments: (a) the lack of a clear understanding of the variation range and time series scale within an individual region, hindering the identification of trend drivers; (b) each region has its own specific range of TWS variation, and identical trend values do not indicate the same level of water stress. For instance, a "−1 mm/yr" trend in water storage may have a minor effect in one region within the range of regional TWS variability, but it could exert significant pressure on another region, surpassing tolerable TWSC. Therefore, relying solely on the magnitude of the trend does not provide comprehensive information on the severity of TWSC. Consequently, we propose a new criterion based on a century-long GRACE-REC data set (Methods section for details) that considers internal climate variability. This criterion helps us understand the degree of TWSC when combined with GRACE trends.

In summary, the objectives of this study were as follows: (a) to estimate the trend bounds of long-term water storage induced by internal climate variability over a fixed time period using a century-long GRACE-REC data set; (b) to verify the reliability of these trend bound estimates and our method; and (c) to apply our method to assess the degree of GRACE trends, precipitation-induced (PI) trends, and non-precipitation-induced (NPI) trends during the GRACE era. TWS changes can be attributed to natural variability, climate change, and anthropogenic influences (An et al., 2021; Zhong, Bai, et al., 2023). Here, we utilize GRACE observations, GRACE-REC data, and other supplementary data sets to provide an integrated attribution of the TWS trends. The PI TWS trend is estimated from the GRACE-REC data set (Humphrey & Gudmundsson, 2019), and the NPI TWS trend is determined by subtracting the PI TWS trend from the GRACE trend. This separation of the GRACE trend enables us to understand different contributions to TWS change. GRACE-FO data is also utilized to analyze the impact of using different windows to evaluate TWS trends. We selected and studied 266 global basins (Figure S1 in Supporting Information S1), but due to the coarse spatial resolution of GRACE data, our focus is on analyzing the driving mechanisms of trends in global large basins (areas $\geq$ 500,000 km^2) (Scanlon et al., 2016). Additionally, we analyze trends in several basins further using precipitation and evapotranspiration (ET) data.

Table 1
Collection of All Data Sets for This Study

Data set	Time span	Spatial	Temporal	Access
JPLM_RL06	April 2002–December 2021	0.5°	Monthly	https://grace.jpl.nasa.gov
GRACE-REC/JPL-GSWP3	1901–2014	0.5°	Monthly	https://doi.org/10.6084/m9.figshare.7670849
GRACE-REC/JPL-MSWEP	1979–2016			
Global major river basins	–	–	–	https://www.bafg.de/SharedDocs/ExterneLinks/GRDC/mrb_shp_zip.html
MSWEP	1980–2016	0.5°	Daily	http://www.gloh2o.org/mswep/
GLEAM_v3.6a	1980–2016	0.25°	Monthly	https://www.gleam.eu/
RGI 6.0	2017	–	–	https://www.glims.org/RGI/rgi60_dl.html
Glacier mass loss data set	2003–2016	0.5°	Monthly	https://doi.org/10.6096/13
Global map of irrigation areas	2013	5'	–	https://www.fao.org/aquastat/en/geospatial-information/global-maps-irrigated-areas/
ISIMIP	1861–2099	0.5°	Monthly	https://www.isimip.org/outputdata/
ICE-5G (VM2)	–	0.5°	–	https://podaac-tools.jpl.nasa.gov/
ICE-6G_D (VM5a)				

2. Data and Methods

2.1. Data

The data can be broadly classified into five categories: GRACE mascon data, GRACE-REC data, boundaries of global major river basins, precipitation and ET data, and ancillary data. Please refer to Table 1 for the specific acquisition of the data sets.

2.1.1. GRACE Data

The JPL mascon RL06_v02 (JPLM_RL06) is used to estimate the TWS trend considering that every 3° mascon is relatively uncorrelated (Rodell et al., 2018) and available GRACE-REC data (Humphrey & Gudmundsson, 2019). The mascon grid is sampled at 0.5° resolution for further application. The GRACE mascon data from JPL have been used that do not require any post-processing steps (Watkins et al., 2015). We refer the readers to Wiese et al. (2016, 2019) for more details about JPL mascons. The period of January 2003 to December 2016 is extracted for TWS trend estimates.

2.1.2. GRACE-REC Data

GRACE-REC data set published by Humphrey and Gudmundsson (2019) is generated by using a statistical relation between daily precipitation, temperature, and detrended and deseasonalized TWS. The model formulation is primarily inspired by the basic principles of hydrological modeling. During the training process, the trends of GRACE TWS and temperature are removed, while the potential TWS trends caused by long-term precipitation are not eliminated in the published GRACE-REC data set (Humphrey & Gudmundsson, 2019). Therefore, the GRACE-REC data set can be utilized to evaluate precipitation-induced (PI) TWS trends. The reconstructed TWSA, with a spatial resolution of 0.5° and temporal scales ranging from days to months, is based on two GRACE processing centers (JPL and GSFC) and three meteorological forcing time series (Multi-Source Weighted-Ensemble Precipitation [MSWEP], ERA5, and Global Soil Wetness Project Phase 3), resulting in six groups GRACE-REC data set (Humphrey & Gudmundsson, 2019). This study uses two GRACE-REC data sets (i.e., JPL-GSWP3 (1901–2014) and JPL-MSWEP (1979–2016)). The century-long JPL-GSWP3 data is used to estimate the upper and lower bounds of TWS trends under natural conditions. Since the JPL-MSWEP data is not available beyond 2016, the JPL-MSWEP data is used to derive the PI trend for the period 2003–2016. The GRACE-REC JPL-MSWEP data is expected to provide the most accurate estimate for the time of 1979–2016 (Humphrey & Gudmundsson, 2019).

2.1.3. Global Major River Basins

The Global Runoff Data Centre (GRDC) serves 520 major river basins throughout the world, with complete citation and reference to incorporated data from the HydroSHEDS database. However, we only select 266 basins with an area larger than 40,000 km^2, which are divided into different size classes: large (40 basins, ≥500,000 km^2), medium (81 basins, 100,000–500000 km^2), and small (145 basins, 40,000–100,000 km^2) (Scanlon et al., 2016).

2.1.4. Precipitation and ET Data

Following the analysis from Rodell et al. (2018) and An et al. (2021), we calculate the mean annual precipitation change based on the MSWEP data set for the periods 2003–2016 and 1980–2016 (precipitation climatology), hereafter referred to as APC_{0316}. The precipitation anomaly (PA) relative to 1980–2016 mean is calculated. Additionally, we determine the changes in ET based on the Global Land Evaporation Amsterdam Model (GLEAM) data set between 2003-2016 and 1980–2016 (ET climatology), hereafter expressed as $AETC_{0316}$. The ET anomaly (ETA) relative to 1980–2016 mean is calculated, and we also calculate the net water flux anomaly (i.e., PA-ETA). The ET from GLEAM is selected considering that the MSWEP precipitation is its forcing data. It is assumed that precipitation and ET remain in dynamic equilibrium under normal conditions. According to the water balance equation (Equation 1), if the mean annual precipitation (2003–2016) exceeds the normal situation, it would contribute to a positive TWS anomaly, while lower precipitation may lead to a negative TWS anomaly. The impact of ET on TWS is the opposite concerning precipitation.

$$\Delta S = P - ET - Q \quad (1)$$

ΔS is the changes in TWS over a specific period, P is precipitation, ET is evapotranspiration, and Q is streamflow (Bai et al., 2022).

2.1.5. Ancillary Data

This study utilizes multi-source auxiliary data sets to analyze the driving mechanisms of trends. To investigate the impact of glacier mass changes on TWSA trends, we utilized the Randolph Glacier Inventory (RGI 6.0) glacier outline and glacier mass change data. The global map of irrigation areas data, published by the Food and Agriculture Organization of the United Nations, was used to study the effect of water use on water storage depletion. Water use data collected by the Inter-Sectoral Impact Model Intercomparison Project was also investigated to study the irrigation, industrial, and domestic water use in these basins. Additionally, glacial isostatic adjustment (GIA) models (ICE-6G_D (VM5a) and ICE-5G (VM2)) used for corrections to JPLM_RL06 and JPLM_RL05 products, respectively, were utilized to discuss the possible sources of uncertainty in GRACE trends.

Most data sets have a resolution of 0.5° × 0.5°, and the other data sets with different resolutions are resampled to 0.5° × 0.5° to further extract the basin-average estimates.

2.2. Methods

It is hard to evaluate the changes in TWS in a basin only relying on the trend value derived from GRACE (referred to as $Trend_G$). To provide a comprehensive understanding of TWS trends over a specific period, we utilize the one century-long GRACE-REC data set as a reference for estimating the upper and lower bounds of natural TWS trends. The upper bound and lower bound of the TWS anomaly trend (hereafter referred to as $Trend_{UB}$ and $Trend_{LB}$) represent the maximum variation of the TWS anomaly trend under natural conditions. By considering $Trend_{UB}$ and $Trend_{LB}$, we can further interpret the TWS anomaly trend for the GRACE era.

The study period spans 14 years during the GRACE era, specifically from 2003 to 2016. The trend derived from GRACE-REC/JPL-MSWEP data for this period (14 years) is used to represent the precipitation-induced (PI) water storage trend (hereafter referred to as $Trend_{PI}$). Additionally, the difference between the $Trend_G$ for 2003–2016 and the $Trend_{PI}$ for the same period is denoted as the non-precipitation-induced (NPI) TWS trend (hereafter referred to as $Trend_{NPI}$). The relationship between these trends is expressed in Equation 2. We calculate the trends for every 14-year period starting from 1901, with a step length of 1 year, based on the JPL-GSWP3 data (i.e., 1901–1914, 1902–1915, …, 2001–2014), resulting in 101 trend series. The maximum (minimum) trend estimate is represented as $Trend_{UB}$ ($Trend_{LB}$).

$$Trend_G = Trend_{PI} + Trend_{NPI} \quad (2)$$

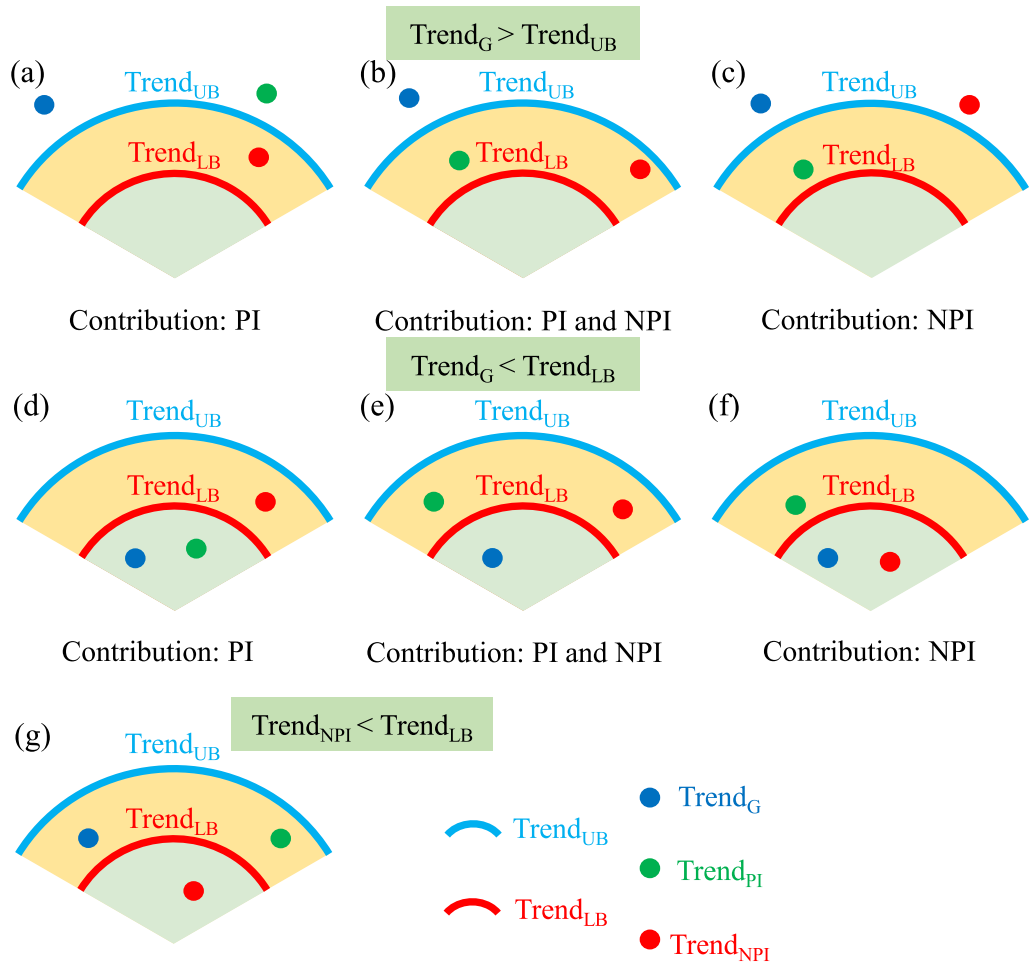

Figure 1. An illustration for the different cases when the $Trend_G$/$Trend_{PI}$/$Trend_{NPI}$ are beyond the $Trend_{UB/LB}$. The blue arc represents the $Trend_{UB}$ and the red arc curves the $Trend_{LB}$ in a basin. The location of points indicates whether the $Trend_G$/$Trend_{PI}$/$Trend_{NPI}$ is beyond $Trend_{UB/LB}$ or not.

The trends of $Trend_G$, $Trend_{PI}$, $Trend_{UB}$, and $Trend_{LB}$ are estimated by least squares fitting (Scanlon et al., 2016), and their uncertainties are one standard deviation (±1σ). The uncertainty of $Trend_{NPI}$ is estimated by error propagation from the uncertainties of $Trend_G$ and $Trend_{PI}$.

Under natural processes without human intervention, the rate of TWS changes should generally fall within the range defined by $Trend_{UB}$ and $Trend_{LB}$. When comparing $Trend_G$ with $Trend_{UB}$ and $Trend_{LB}$ (Figure 1), several typical cases can be observed. First, if $Trend_G$ exceeds $Trend_{UB}$, three scenarios are possible: Case (a), $Trend_{PI}$ is also greater than $Trend_{UB}$, then $Trend_{PI}$ contributes significantly to the increase in TWS (Figure 1a); Case (b), both $Trend_{PI}$ and $Trend_{NPI}$ are less than $Trend_{UB}$, and they jointly contribute to a significant TWS increase (Figure 1b); Case (c), $Trend_{NPI}$ exceeds $Trend_{UB}$ (Figure 1c), suggesting that the TWS trends are primarily caused by $Trend_{NPI}$. Conversely, if $Trend_G$ is lower than $Trend_{LB}$, indicating severe TWS depletion, three scenarios are typically observed: Case (d), $Trend_{PI}$ is also less than $Trend_{UB}$, and $Trend_{PI}$ contributes to this water storage depletion (Figure 1d); Case (e), both $Trend_{PI}$ and $Trend_{NPI}$ are greater than $Trend_{LB}$, leading to a significant TWS decline (Figure 1e); and Case (f), $Trend_{NPI}$ is lower than $Trend_{UB}$ (Figure 1f), indicating that the TWS trends are likely caused by $Trend_{NPI}$. Additionally, there is also a case where $Trend_{NPI}$ is below $Trend_{LB}$, while $Trend_G$ and $Trend_{PI}$ fall within the range defined by $Trend_{UB}$ and $Trend_{LB}$ (Figure 1g). In such a case, potential non-precipitation-induced factors, including glacier melt, groundwater withdrawal, and increased ET, can contribute to TWS loss, which may be difficult, or even impossible, to recover. It should be noted that Figure 1 includes most cases in this study, but not all possible scenarios.

To further demonstrate our method, we present five typical basins in Figure S2 in Supporting Information S1. The $Trend_{UB}$ and $Trend_{LB}$ are clearly observed over the century-long period. Moreover, the severity of $Trend_G$ relative to the 100-year trends, as well as the variation characteristics of the trends and time series in individual basins, are clearly visible.

The trend in TWS can be influenced by both precipitation and non-precipitation factors, such as ET, temperature, and human activities. When the $Trend_{PI}$ falls outside the range defined by $Trend_{UB}$ and $Trend_{LB}$, it indicates a significant positive or negative trend in TWS due to precipitation. Similarly, when the $Trend_{NPI}$ falls outside $Trend_{UB}$ or $Trend_{LB}$, it indicates a significant positive or negative trend in TWS due to the non-precipitation factors. It is important to note that the estimation of $Trend_{PI}$ in this study is solely based on JPL-MSWEP data, encompassing the impact of natural variability and long-term climate changes in precipitation (Humphrey & Gudmundsson, 2019). However, $Trend_{PI}$ may not fully capture the contribution of changes in precipitation from 2003 to 2016 relative to the long-term precipitation climatology (1980–2016) in certain basins. For example, if annual precipitation increased by 20 mm each year during 2003–2016 compared to the long-term average, it could disrupt the regional water balance equilibrium and lead to an increase in TWS. However, this change may not be reflected in the reconstructed precipitation-induced TWSA, as the parameters of the reconstruction model remain unchanged. Therefore, further analysis of changes in multi-year mean precipitation is conducted to explain specific TWS trends observed by GRACE in certain basins.

The flowchart depicting our method and the major content is illustrated in Figure 2. The description of abbreviations appearing in the study is presented in Table S2 in Supporting Information S1.

3. Results

3.1. Spatial Distribution of Basins Beyond $Trend_{UB}$ and $Trend_{LB}$

From a global perspective, there are few regions where TWS trends are significantly affected by PI factors (Figure 3). However, evident positive TWS trends driven by precipitation can be observed in the west of the Ganges River Basin, central North America, and southeast South America, while noticeable negative precipitation-induced trends occur in the Don River Basin and northeastern South America (Figure 3b). These regions correspond to the basins shown in Figures 4c and 4d. In contrast, TWS trends in more regions are related to non-precipitation factors (Figure 3c), with specific basins identified in Figures 4e and 4f.

To analyze the spatial distribution of basins with $Trend_G$, $Trend_{PI}$, and $Trend_{NPI}$ beyond the range of $Trend_{UB}$ or $Trend_{LB}$, we present a plot for 266 global basins in Figure 4. Figures 4a and 4b show that more basins experience severe TWS deficits than those with significant TWS increases. Globally, only 10 basins exhibit $Trend_{PI}$ exceeding the $Trend_{UB}$, while only six basins fall below the $Trend_{LB}$ (Figures 4c and 4d). It is understood that since the $Trend_{PI}$ is compared with the century-long range of $Trend_{PI}$. Several basins with $Trend_{NPI}$ exceeding $Trend_{UB}$ are located in northeast America and central Africa (Figure 4e). Most basins with significant negative $Trend_{NPI}$ (Figure 4f) are in the groundwater depletion or glacier regions.

3.2. Comparison of Trends ($Trend_G$, $Trend_{PI}$, $Trend_{NPI}$) With $Trend_{UB}$ and $Trend_{LB}$

To better check the magnitude of the trends ($Trend_G$, $Trend_{PI}$, $Trend_{NPI}$) beyond the range of $Trend_{UB}$ and $Trend_{LB}$ and interpret the severity of these trends to some extent, we plot a scatter plot of the trends ($Trend_G$, $Trend_{PI}$, $Trend_{NPI}$) for 266 basins against the $Trend_{UB}$ and $Trend_{LB}$ (Figure 5). It reveals that most basins exhibit localization within Region B and Region C concerning the $Trend_G$, $Trend_{PI}$, and $Trend_{NPI}$. None of the large basins exceed a deviation of 5 mm/yr above the $Trend_{UB}$, whereas three large basins deviate by 5 mm/yr below the $Trend_{LB}$ (Figure 5a). Specifically, for the $Trend_{PI}$, only one basin, namely the Stikine River Basin, exceeds the $Trend_{UB}$ by 5 mm/yr, and no basin falls below the $Trend_{LB}$ by the same margin. As for the $Trend_{NPI}$, similar to $Trend_G$, no large basin exceeds the $Trend_{UB}$ by 5 mm/yr, but four large basins deviate by 5 mm/yr below the $Trend_{LB}$ (Figure 5c).

3.3. Reliability of the Estimated $Trend_{UB}$ and $Trend_{LB}$

To assess the reliability of $Trend_{UB}$ and $Trend_{LB}$ estimates, we calculated the trends for every 14 years from 1979 to 2014 with a 1-year interval based on GRACE-REC/JPL-MSWEP and JPL-GSWP3 data (Data Set S1).

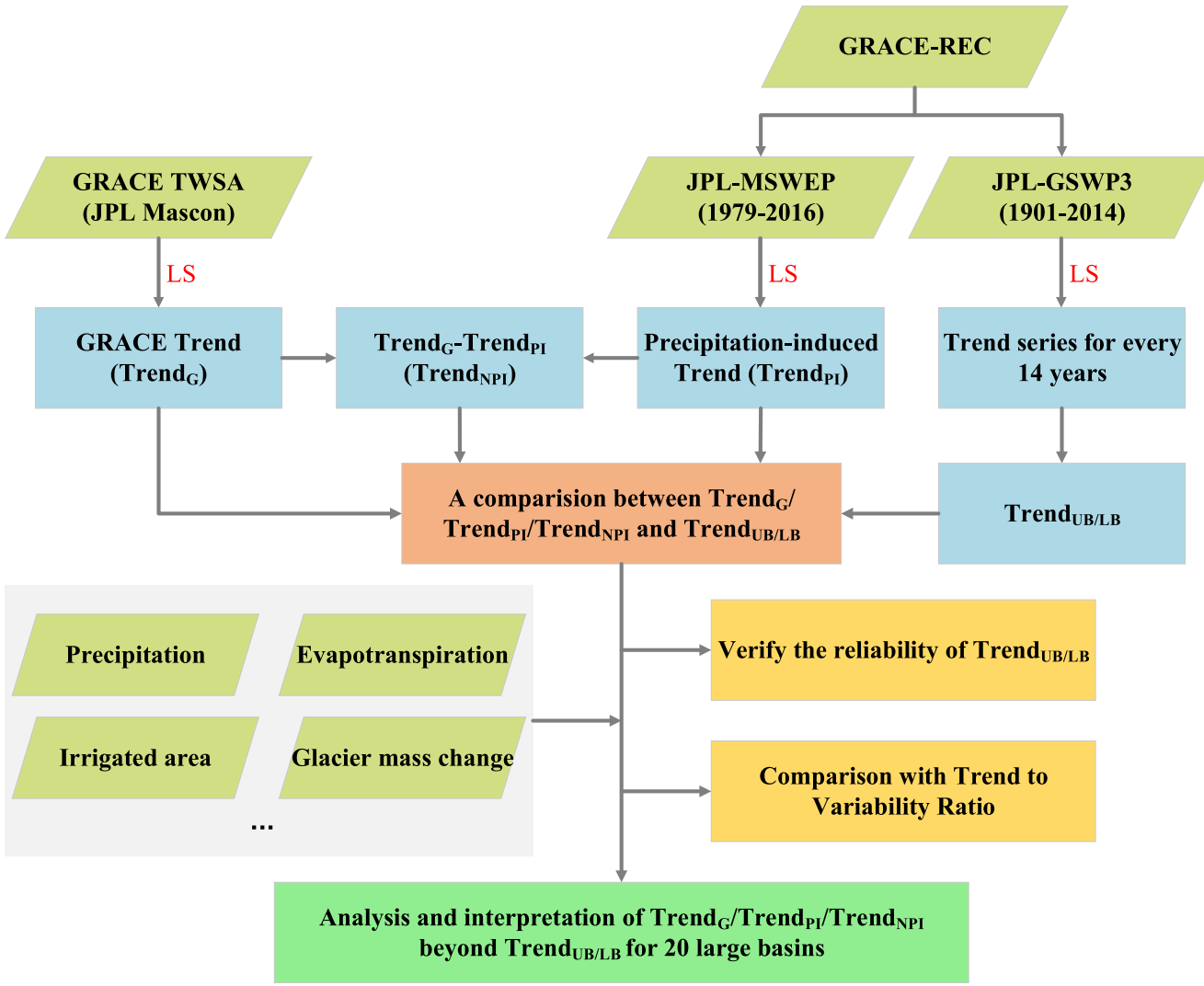

Figure 2. The flow chart of this study.

This calculation resulted in 23 trend series. The bound of the trend series for JPL-MSWEP is expressed as $Trend_{UB(M79\text{-}14)}/Trend_{LB(M79\text{-}14)}$, and for JPL-GSWP3, it is expressed as $Trend_{UB(G79\text{-}14)}/Trend_{LB(G79\text{-}14)}$. The scatter plot in Figure 6a displays the differences between $Trend_{UB(M79\text{-}14)}$ and $Trend_{UB(G79\text{-}14)}$, as well as between $Trend_{LB(M79\text{-}14)}$ and $Trend_{LB(G79\text{-}14)}$, for the global 266 basins. Approximately 76.7% of the global basins exhibit an absolute deviation between $Trend_{UB(M79\text{-}14)}$ and $Trend_{UB(G79\text{-}14)}$ of less than 2 mm/yr, and 70.3% of the basins show an absolute deviation between $Trend_{LB(M79\text{-}14)}$ and $Trend_{LB(G79\text{-}14)}$ of less than 2 mm/yr. Only six basins and nine basins exceed a 2 mm/yr absolute deviation between $Trend_{UB(M79\text{-}14)}$ and $Trend_{UB(G79\text{-}14)}$, and $Trend_{LB(M79\text{-}14)}$ and $Trend_{LB(G79\text{-}14)}$, respectively, among the global 39 arid basins. Thus, the $Trend_{UB}$ and $Trend_{LB}$ estimates from JPL-GSWP3 are considered reliable to some extent.

Figure 6b presents the same information as Figure 6a but for the 54 large and medium basins that extend beyond the bound values. The statistics of the absolute difference values of trend bounds between JPL-MSWEP and JPL-GSWP3 are summarized in Table 2. In most basins, the absolute deviation between $Trend_{UB(G79\text{-}14)}$ and $Trend_{UB(M79\text{-}14)}$, as well as between $Trend_{LB(G79\text{-}14)}$ and $Trend_{LB(M79\text{-}14)}$, is less than 2 mm/yr (Figure 6b), indicating greater consistency compared to the global 266 basins (Figure 6a). Therefore, the analysis of trend bounds in the 54 basins is considered reliable. Notably, there are significant deviations of 8.9, 4.9, and 9.0 mm/yr between $Trend_{UB(M79\text{-}14)}$ and $Trend_{UB(G79\text{-}14)}$ for the humid Cuanza River Basin, semi-arid Kunene River Basin, and Volta River Basin, respectively, and 6.8 mm/yr between $Trend_{LB(M79\text{-}14)}$ and $Trend_{LB(G79\text{-}14)}$ for the semi-arid Okavango River Basin. Further discussions on specific basins listed in Table 2, are presented in Section 4.

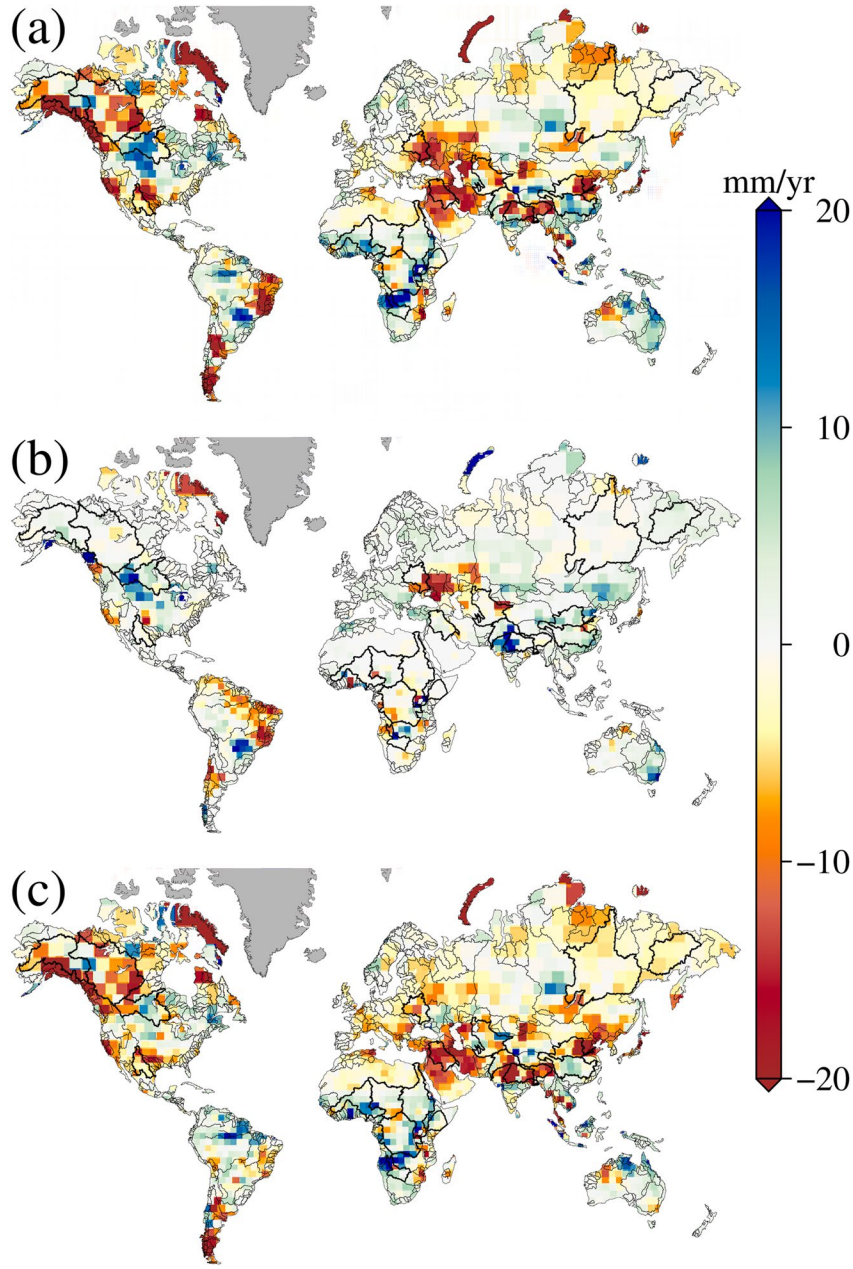

Figure 3. Global grid-scale (a) Gravity Recovery and Climate Experiment, (b) precipitation-induced, and (c) non-precipitation-induced trends map from 2003 to 2016 based on JPLM and GRACE-REC/JPL-MSWEP. The boundaries of 20 large basins analyzed in this study are bold.

3.4. Comparison With Trend to Variability Ratio

Vishwakarma et al. (2021) proposed a metric called the trend to variability ratio (TVR) to assess the intensity of GRACE TWS trends. The TVR is defined as the multi-year TWS trend multiplied by the corresponding number of years and divided by the standard deviation of multi-decadal TWS natural interannual variability from GRACE-REC. Our method identifies most of the basins that are also identified by the TVR metric (Table 3 and Table S4 in Supporting Information S1). For basins such as the Kolyma, Lake Chad, and Jubba River Basin, the TVRs fall within the range of −2 to 2, indicating no significant trend, as the values of Trend_G are small. However, the Trend_G or Trend_{NPI} exceeds the $\text{Trend}_{UB/LB}$, which are also small in magnitude.

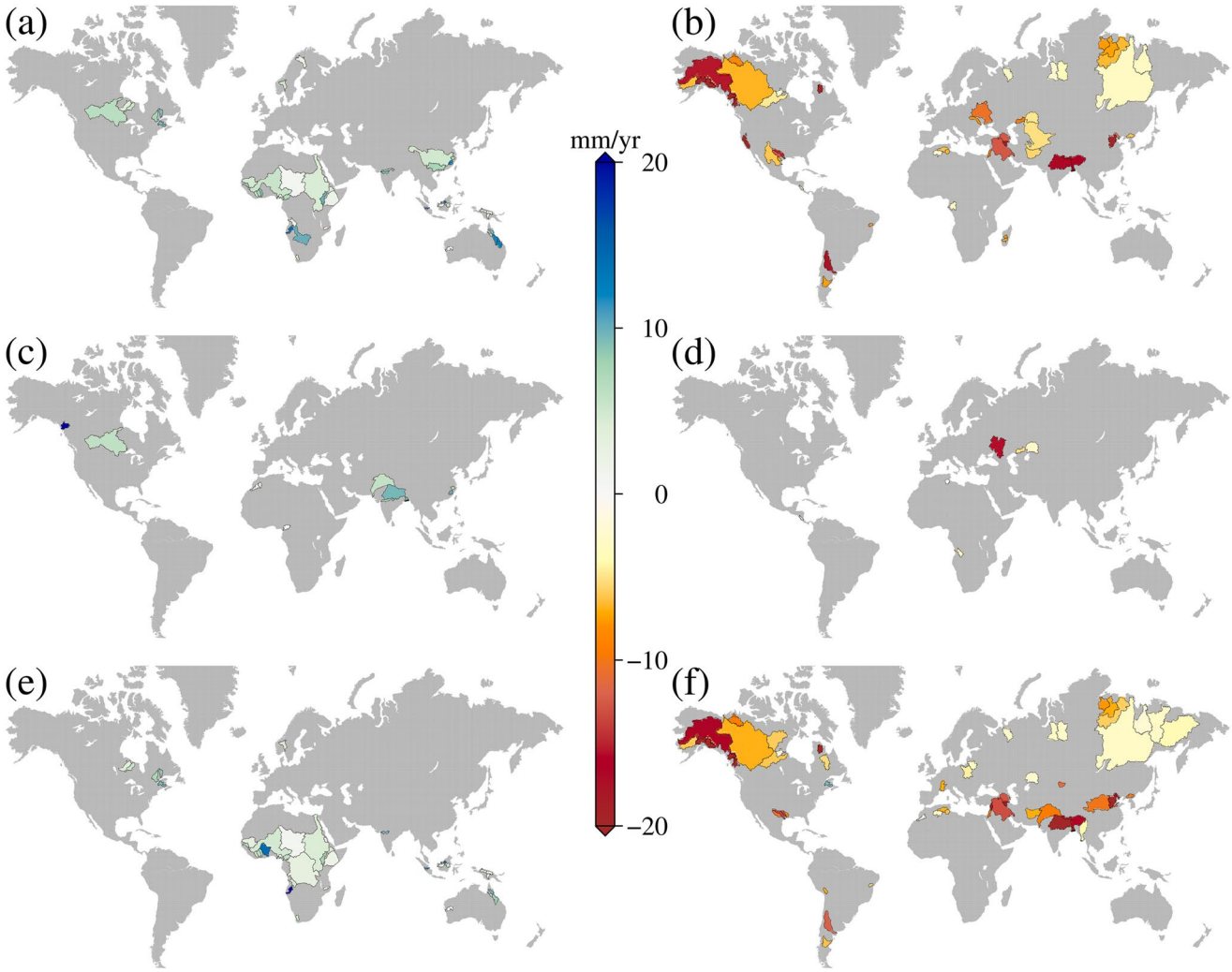

Figure 4. Spatial distribution of global basins beyond $Trend_{UB}$ and $Trend_{LB}$. (a) $Trend_G$ of 45 basins (16.9%) exceeds the $Trend_{UB}$, (b) $Trend_G$ of 50 basins (18.8%) is below the $Trend_{LB}$, (c) $Trend_{PI}$ of 10 basins (3.8%) exceeds the $Trend_{UB}$, (d) $Trend_{PI}$ of 6 basins (2.3%) is below the $Trend_{LB}$, (e) $Trend_{NPI}$ of 38 basins (14.3%) exceeds the $Trend_{UB}$, and (f) $Trend_{NPI}$ of 55 basins (20.7%) is below the $Trend_{LB}$.

While the TVR method considers the standard deviation of internal variability, our method assesses the maximum and minimum trends induced by the internal climate variability of one-century water storage. In cases where a catchment experiences large magnitude decadal cycles, the TVR method may not flag the trend as significant. Our method, on the other hand, improves upon TVR by providing a better understanding of the severity of trends observed during the 14-year GRACE period relative to changes in interannual variability over the same period. Additionally, both components of $Trend_G$, namely $Trend_{PI}$, and $Trend_{NPI}$, are used to determine if a basin falls beyond the $Trend_{UB/LB}$. Therefore, in some basins, $Trend_{PI}$ and $Trend_{NPI}$ exceed the $Trend_{UB/LB}$ and are flagged, while TVRs remain within −2 to 2. Examples of such basins include the Kolyma, Indigirka, Pur, Vistula, Caniapiscau, and Cuanza River Basin. These basins are highlighted by bold or underlined text as the contributions of PI and NPI factors to the GRACE TWS trend are in opposite directions.

4. Trend Analysis of Global Large Basins

Trend estimates ($Trend_{UB}$, $Trend_{LB}$, $Trend_G$, $Trend_{PI}$, and $Trend_{NPI}$) for global 266 basins are presented in Data Set S2. Global 20 large basins with one of $Trend_G$, $Trend_{PI}$, and $Trend_{NPI}$ beyond the $Trend_{UB}$ or $Trend_{LB}$ are analyzed. The trend estimates for these 20 basins are provided in Table 3. The basins have been sorted and analyzed based on their respective continents. The location of 20 basins is presented in Figure 3 and numbered in Figure S1 in Supporting Information S1.

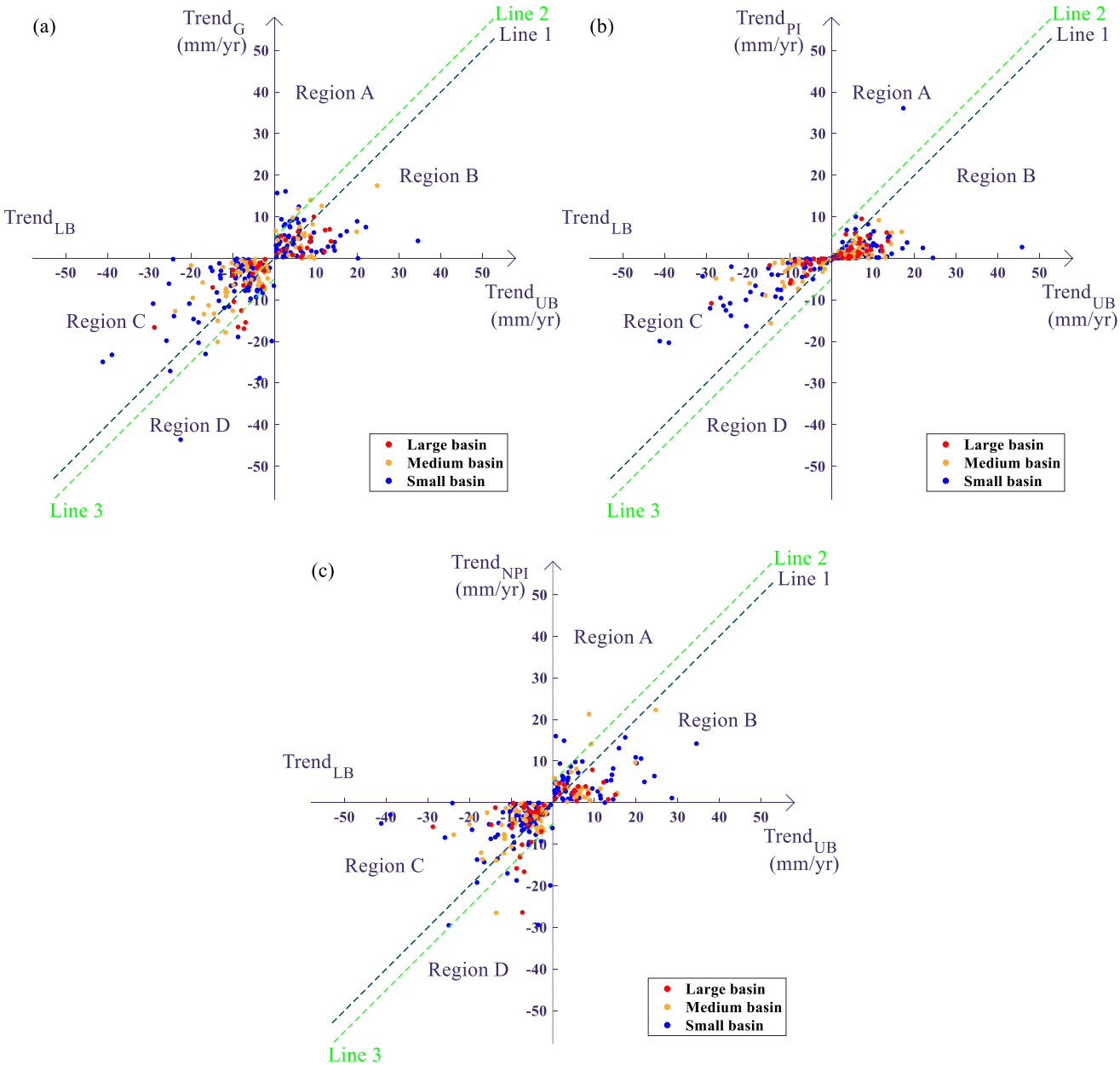

Figure 5. Scatter plots depicting the relationships between $Trend_G$, $Trend_{PI}$, $Trend_{NPI}$, $Trend_{UB}$, and $Trend_{LB}$. The red dots represent large basins, the yellow dots represent medium basins, and the blue dots represent small basins. Regions A-D are defined by the coordinate axis and diagonal line (Line 1). Region A represents basins where $Trend_G$ is positive and exceeds the $Trend_{UB}$, Region B represents basins where $Trend_G$ is positive but below the $Trend_{UB}$, Region C represents basins where $Trend_G$ is negative but above the $Trend_{LB}$, and Region D represents basins where $Trend_G$ is negative and below the $Trend_{LB}$. Basins in Regions A and D are analyzed in this study. If the points lie above Line 2 or below Line 3, there may be significant changes in the terrestrial water storage of the corresponding basins. It should be noted that the dot for the Copper River Basin is not shown in panels (a, c) because of the extreme trends ($Trend_G$: −156.5 mm/yr and $Trend_{NPI}$: −159.2 mm/yr). The dot for the Stikine River Basin does not appear in panel (c) to improve clarity as it has a significant trend ($Trend_{NPI}$: −79.7 mm/yr).

4.1. Eurasia

The Yellow River Basin has experienced continuous and severe TWS depletion ($Trend_G$: -6.5 ± 0.7 mm/yr) from 2003 to 2016 due to climate change and anthropogenic activities. The region experiencing significant water loss is primarily located in the middle and lower reaches of the Yellow River Basin, adjacent to the research hotspot for water storage depletion in the North China Plain (Long et al., 2020). The APC_{0316} for this period is 21.3 mm, and the precipitation trend from 2003 to 2016 is 5.6 mm/yr (Table S5 in Supporting Information S1), resulting in a positive $Trend_{PI}$ of 3.6 ± 0.2 mm/yr. Consequently, the $Trend_{NPI}$ (-10.1 ± 0.7 mm/yr) is significantly lower than

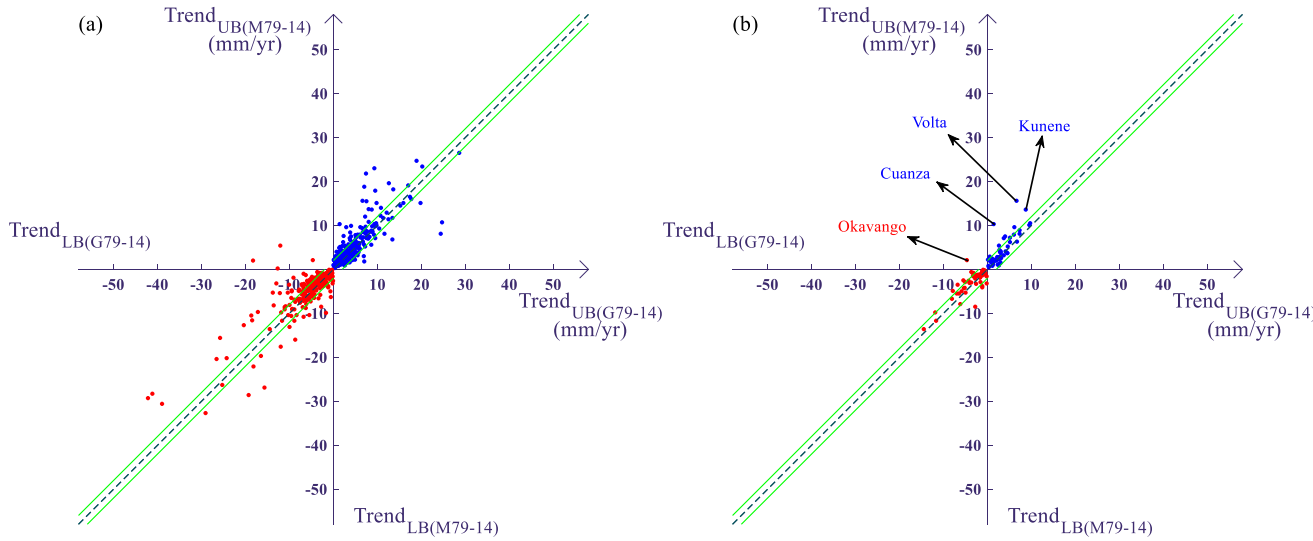

Figure 6. Scatter plots of the bound values of trends for every 14 years starting from 1979 with a 1-year interval during 1979–2014 based on Gravity Recovery and Climate Experiment-REC/JPL-MSWEP and JPL-GSWP3, respectively. Blue dots represent the differences between $Trend_{UB(M79-14)}$ and $Trend_{UB(G79-14)}$, corresponding to 266 basins. Red dots represent the differences between $Trend_{LB(M79-14)}$ and $Trend_{LB(G79-14)}$, corresponding to 266 basins. Dots between the two green lines indicate basins where the trend differences between $Trend_{UB(M79-14)}$ and $Trend_{UB(G79-14)}$ or between $Trend_{LB(M79-14)}$ and $Trend_{LB(G79-14)}$ are less than 2 mm/yr. Panel (b) presents the same information as panel (a), but panel (b) corresponds to 54 large/medium basins beyond the bound values. Note: The Stikine River Basin is not shown in panel (a) because of the significant differences between $Trend_{UB(M79-14)}$ (69.9 mm/yr) and $Trend_{UB(G79-14)}$ (17.3 mm/yr), which indicates that there may exist a large uncertainty in the estimate of $Trend_{UB}$ and $Trend_{LB}$ for this basin.

the $Trend_{LB}$. The negative $Trend_{NPI}$ is attributed to increased irrigation water withdrawals (Figures S3a and S4 in Supporting Information S1) and reservoir operation (Xie et al., 2019). Additionally, the $AETC_{0316}$ is 20.4 mm, and the trend of annual ET from 2003 to 2016 is 2.0 mm/yr (Table S5 in Supporting Information S1), which partly contributes to the NPI water storage depletion.

In the Yangtze River Basin, the $Trend_G$ (4.9 ± 0.9 mm/yr) slightly exceeds the $Trend_{UB}$ (4.7 ± 0.4 mm/yr), with the $Trend_{PI}$ (2.7 ± 0.3 mm/yr) accounting for 55.1% of the $Trend_G$. The PA and PA-ETA both show significant positive values in the latter 2 years (Figure S5b in Supporting Information S1). The primary increase in TWS is observed in the middle reaches of the Yangtze River Basin, as depicted in Figure 3a. Additionally, the upward trend in precipitation-induced TWS is observed in the southern and eastern regions of the basin. On the other hand, the $Trend_{NPI}$ exhibits an increase in the middle part of the Yangtze River Basin (Figure 3c), particularly in proximity to the Three Gorges Dam (TGD). It is noteworthy that the construction of the TGD occurred during the study period. According to the Department of Water Resources of Hubei Province, the maximum reservoir capacity of TGD was 39.3 km^3 in 2016, which, considering the total basin area, can contribute to an increase in water storage of approximately 22.5 mm, resulting in a mean trend of 1.6 mm/yr for 2003–2016. Therefore, the construction of TGD can explain most of the NPI trends (i.e., 2.2 ± 0.9 mm/yr). Moreover, groundwater seepage from dams, glaciers melting in the source area of the Yangtze River, and measures for protecting the Yangtze River would also affect NPI TWS (Chao et al., 2021).

Table 2
Statists of Absolute Difference Values Between $Trend_{UB(M79-14)}$ and $Trend_{LB(M79-14)}$; and Between $Trend_{UB(G79-14)}$ and $Trend_{LB(G79-14)}$ for the 54 Basins

	Number of basins		
Absolute differences	>5 mm/yr	>3 mm/yr	>2 mm/yr
$Trend_{UB(M79-14)}$ versus $Trend_{UB(G79-14)}$	2	6	10
$Trend_{LB(M79-14)}$ versus $Trend_{LB(G79-14)}$	2	4	13

Note. Between $Trend_{UB(M79-14)}$ and $Trend_{UB(G79-14)}$, basins with absolute difference values of more than 2 mm/yr are listed in Table S2 in Supporting Information S1. Between $Trend_{LB(M79-14)}$ and $Trend_{LB(G79-14)}$, basins with absolute difference values of more than 2 mm/yr are shown in Table S3 in Supporting Information S1.

The Brahmaputra River Basin is experiencing continuous glacier melting upstream and severe groundwater loss downstream ($Trend_G$: −16.5 ± 1.1 mm/yr; $Trend_{NPI}$: −15.8 ± 1.1 mm/yr). The precipitation-induced TWS anomaly fluctuates around zero and shows a small trend. $Trend_{NPI}$ accounts for the majority of $Trend_G$ (95.8%), and both are approximately twice the $Trend_{LB}$ (−8.7 mm/yr). The glacier mass loss rate accounts for 63.0% of $Trend_G$ (Table S6 in Supporting Information S1). The irrecoverable nature of TWS loss is evident in this basin. The combined factors of snow and glacier shrinkage, concentrated population, agricultural irrigation, and possible signal leakage of groundwater deficit from the Ganges River Basin due to the

Table 3
Statistics for the 20 Large Basins Exceeding the Trend Bounds, Including Different Trend Estimates ($Trend_G$, $Trend_{PI}$, $Trend_{NPI}$) and Trend to Variability Ratio, Along With Their Respective Uncertainties

Continent	ID	Basin	$Trend_{LB}$	$Trend_{UB}$	$Trend_G$	$Trend_{PI}$	$Trend_{NPI}$	TVR	Area
Eurasia	1	Yellow River	−7.4 ± 0.4	6.8 ± 0.4	**−6.5 ± 0.7**	**3.6 ± 0.2**	**−10.1 ± 0.7**	−6.1 ± 0.7	96.3
	2	Yangtze	−5.3 ± 0.4	4.7 ± 0.4	4.9 ± 0.9	2.7 ± 0.3	2.2 ± 0.9	4.5 ± 0.8	174.8
	3	Brahmaputra	−8.7 ± 0.7	8.1 ± 0.8	−16.5 ± 1.1	−0.7 ± 0.3	−15.8 ± 1.1	−14.0 ± 1.0	54.1
	4	Ganges	−7.3 ± 0.7	7.3 ± 0.7	**−16.9 ± 2.2**	**9.5 ± 0.7**	**−26.4 ± 2.3**	−5.6 ± 0.7	100.7
	5	Indus	−5.2 ± 0.4	3.5 ± 0.3	**−3.7 ± 1.1**	**5.8 ± 0.4**	**−9.5 ± 1.2**	−2.0 ± 0.6	86.5
	6	Aral Sea	−5.0 ± 0.2	5.0 ± 0.4	−5.1 ± 1.0	−2.8 ± 0.4	−2.3 ± 1.1	−3.1 ± 0.6	137.3
	7	Shatt Al Arab	−7.9 ± 0.5	6.3 ± 0.5	**−12.6 ± 1.4**	**0.5 ± 0.6**	**−13.1 ± 1.5**	−4.8 ± 0.6	93.6
	8	Dnieper	−9.7 ± 0.8	11.1 ± 0.7	−10.4 ± 1.5	−5.3 ± 0.5	−5.1 ± 1.6	−4.5 ± 0.7	51.0
	9	Kolyma	−3.7 ± 0.3	4.0 ± 0.4	**−1.7 ± 1.0**	**2.0 ± 0.4**	**−3.7 ± 1.1**	−1.1 ± 0.7	65.3
	10	Lena	−2.4 ± 0.3	2.6 ± 0.2	−3.0 ± 1.0	−0.1 ± 0.3	−2.9 ± 1.0	−2.6 ± 0.9	245.4
North America	11	Yukon	−6.9 ± 0.3	6.9 ± 0.4	**−15.4 ± 1.1**	**1.2 ± 0.4**	**−16.6 ± 1.2**	−9.2 ± 0.7	83.3
	12	Mackenzie	−2.7 ± 0.2	3.9 ± 0.2	**−6.8 ± 0.7**	**0.1 ± 0.1**	**−6.9 ± 0.7**	−8.1 ± 0.9	179.6
	13	Nelson	−4.5 ± 0.3	5.7 ± 0.5	6.4 ± 1.4	6.0 ± 0.5	0.4 ± 1.5	3.2 ± 0.7	110.7
	14	Rio Grande	−6.0 ± 0.2	2.9 ± 0.2	−6.1 ± 1.1	−0.6 ± 0.4	−5.5 ± 1.2	−3.8 ± 0.7	67.4
Africa	15	Niger	−1.4 ± 0.1	1.6 ± 0.1	5.4 ± 0.6	0.7 ± 0.1	4.7 ± 0.6	8.2 ± 1.0	212.3
	16	Chad	−1.5 ± 0.1	0.6 ± 0.1	0.9 ± 0.5	0.0 ± 0.1	0.9 ± 0.5	1.3 ± 0.8	247.1
	17	Nile	−1.7 ± 0.2	2.7 ± 0.2	4.4 ± 0.8	0.1 ± 0.2	4.3 ± 0.8	5.6 ± 1.0	335.3
	18	Jubba	−1.8 ± 0.2	1.6 ± 0.2	1.9 ± 0.7	−0.1 ± 0.2	2.0 ± 0.7	1.8 ± 0.7	79.8
	19	Congo	−3.0 ± 0.1	2.9 ± 0.2	2.3 ± 1.2	−0.9 ± 0.3	3.2 ± 1.2	2.4 ± 1.2	370.5
	20	Okavango	−10.1 ± 0.4	9.5 ± 0.5	10.0 ± 2.0	2.1 ± 0.8	7.9 ± 2.2	4.2 ± 0.9	69.2

Note. Bold values indicate cases where a positive PI trend results in a negative GRACE trend, indicating severe water loss basins. Underlined values indicate cases where a negative PI trend is accompanied by a positive GRACE trend, indicating significant water gain basins. The unit of trend is mm/yr, and the unit of area is 10^4 km^2.

mismatch between basin boundary and mascon grids (X. Chen et al., 2017; Scanlon et al., 2018; Vishwakarma et al., 2016, 2021) can explain this.

The depletion of TWS in the Ganges River Basin in northern India has been a prominent research topic (Rodell et al., 2018; Vishwakarma et al., 2021). The trends ($Trend_G$: −16.9 ± 2.2 mm/yr, $Trend_{NPI}$: −26.4 ± 2.3 mm/yr) are significantly lower than the $Trend_{LB}$ (−7.3 mm/yr), and the glacier mass loss rate only accounts for a small part (18.2%) of $Trend_G$. The interannual fluctuation of TWSA can be well explained by precipitation, thus the NPI TWSA shows a continuous decline (Figure 7d). Non-precipitation factors have a more significant effect on the TWS in the Ganges River Basin, despite the annual precipitation trend showing a rate of 4.7 mm/yr (2003–2016). The TWS loss in the Ganges River Basin is likely to be irrecoverable, with anthropogenic groundwater extraction for agricultural irrigation (Figure S4b in Supporting Information S1) being the main reason for the decline.

In the Indus River Basin, the $Trend_{NPI}$: −9.5 ± 1.2 mm/yr is below the $Trend_{LB}$ (−5.2 ± 0.4 mm/yr). The major increase in PI TWS and decrease in NPI TWS are both located in the upstream region in this basin (Figure 3). The glacier mass loss rate is larger than $Trend_G$ (Table S6 in Supporting Information S1), and it accounts for about half of the $Trend_{NPI}$, and the water storage depletion also resulted from groundwater withdrawals to support irrigated agriculture and rapid population growth (Zhu et al., 2021). Interestingly, the $Trend_{PI}$ (5.8 ± 0.4 mm/yr) also exceeds the $Trend_{UB}$ (3.5 ± 0.3 mm/yr) and $Trend_{UB(M79\text{-}14)}$ (4.1 ± 0.3 mm/yr), indicating that the actual water depletion caused by non-precipitation-induced factors is significantly greater than the GRACE observations, with a significantly increased contribution from precipitation (24.3 mm/yr, 2003–2016 and APC_{0316} is 61.4 mm) (Table S5 in Supporting Information S1) in this basin.

In the Aral Sea Basin, the $Trend_G$ (−5.1 ± 1.0 mm/yr) is slightly below the $Trend_{LB}$ (−5.0 ± 0.2 mm/yr). The significant decline occurs in the glacial regions (Figures S6a and S6c in Supporting Information S1), which serve

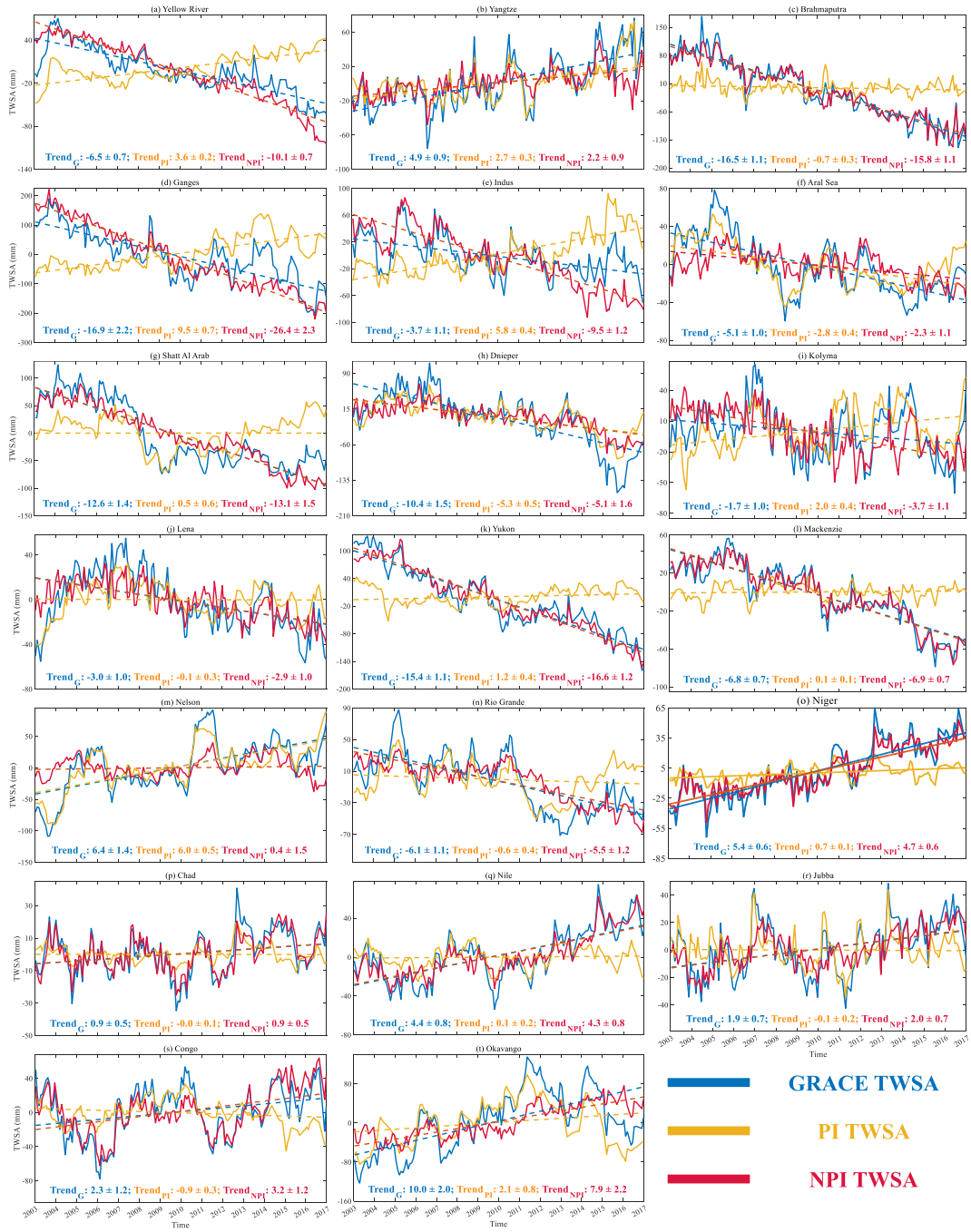

Figure 7. Time series of Gravity Recovery and Climate Experiment (GRACE) TWSA from JPLM, PI TWSA from GRACE-REC/JPL-MSWEP, and NPI TWSA in global 20 large basins from 2003 to 2016. The NPI TWSAs are estimated from GRACE minus PI TWSAs.

as the source of the Syr Darya River. The $Trend_{PI}$ (-2.8 ± 0.4 mm/yr) and $Trend_{NPI}$ (-2.3 ± 1.1 mm/yr) account for 54.9% and 45.1% of the $Trend_G$, respectively. Both the PI and NPI factors contribute to a significant decrease in TWS. Specifically, from 2003 to 2011, the decline in precipitation contributes to the decrease in TWS, with the two time series showing a similar trend. However, after 2011, non-precipitation factors lead to the decrease (Figure 7f). The Aral Sea has been shrinking since the 1960s due to irrigation projects in the Soviet Union that diverted water away from the sea (Shi et al., 2014; Yao et al., 2023). The Aral Sea Basin has experienced reduced surface runoff and increased ET (Table S5 in Supporting Information S1) due to excessive irrigation and

industrial water use (Figure S3 in Supporting Information S1), as well as rising temperatures, all of which have played a major role in TWS loss.

Both the grid-scale TWS trend map (Figure 3a) and the catchment-scale TWS trend map (Figure 4f) show a severe trend of water loss in the arid Shatt Al Arab River Basin. Both $Trend_G$ and $Trend_{NPI}$ are much lower than the $Trend_{LB}$ (-7.9 ± 0.5 mm/yr), indicating that the depletion of water resources in the Shatt Al Arab River Basin is irrecoverable. The $Trend_G$ is -12.6 ± 1.4 mm/yr, and $Trend_{NPI}$ (-13.1 ± 1.5 mm/yr) primarily contributes to the depletion of TWS, while the precipitation only contributes slightly to an increase in TWS. The interannual fluctuations in TWS can mostly be explained by the PI TWS, while the NPI TWS shows a continuous decline (Figure 7g). The construction of dams in the upstream and transboundary water politics have resulted in reduced downstream water availability (Rodell et al., 2018; Voss et al., 2013). Additionally, agricultural irrigation and domestic water demand (Figures S3a and S4 in Supporting Information S1) exert severe pressure on groundwater resources (Chao et al., 2018; Joodaki et al., 2014). The APC_{0316} value of -14.7 mm (accounting for 4.2% of total precipitation from 1980 to 2016) (Table S5 in Supporting Information S1) may also contribute to the decline in TWS.

Ukraine is often referred to as the breadbasket of Europe, with 80.0% of its water resources coming from the Dnieper River Basin (Davybida & Kuzmenko, 2018). Pumping groundwater for agricultural irrigation and industrial water use may be the primary reason for groundwater loss (Figure S3 in Supporting Information S1). The $Trend_{PI}$ (-5.3 ± 0.5 mm/yr), which is close to the $Trend_{LB(M79\text{-}14)}$ (-5.5 ± 0.6 mm/yr), and the $Trend_{NPI}$ (-5.1 ± 1.6 mm/yr) jointly contribute to severe TWS loss ($Trend_G$: -10.4 ± 1.5 mm/yr) in the Dnieper River Basin (Figure 7h). Approximately half of Ukraine's population lives near the Dnieper River Basin, and two-thirds of the population depends on the Dnieper River for drinking water (Pichura et al., 2020). The high population density exerts tremendous pressure on the TWS of the Dnieper River Basin. Additionally, the $AETC_{0316}$ value is 20.3 mm (Table S5 in Supporting Information S1), and increased ET may be a result of water storage depletion.

Located at high latitudes, the Kolyma River Basin is entirely covered by continuous permafrost, the mass anomalies in this basin are mainly controlled by snow-mass variations (Suzuki et al., 2021). The $Trend_{PI}$ is 2.0 ± 0.4 mm/yr, and this basin shows a positive trend of precipitation (6.5 mm/yr), with a significant APC_{0316} value of 34.4 mm (accounting for 7.0% of the mean annual precipitation for 1980–2016) (Table S5 in Supporting Information S1). However, under global warming conditions, snow mass loss and extensive permafrost melting contribute to the negative TWS trend (-1.7 ± 1.0 mm/yr) in this basin, and this is why the $Trend_{NPI}$ (-3.7 ± 1.1 mm/yr) is close to the $Trend_{LB}$ (-3.7 ± 0.3 mm/yr).

The Lena River Basin with a large area (245.4×10^4 km^2), is experiencing an overall decreasing trend (-3.0 ± 1.0 mm/yr) that exceeds the $Trend_{LB}$ (-2.4 ± 0.3 mm/yr). The PI TWSA increased from 2003 to 2007 and then fluctuated around the mean value. The APC_{0316} value is 25.0 mm (Table S5 in Supporting Information S1), indicating more precipitation from 2003 to 2016, although there is a slight declining trend in precipitation (-0.5 mm/yr). This results in a negative $Trend_{PI}$ (-0.1 ± 0.3 mm/yr). The $AETC_{0316}$ value is 12.5 mm, and there is a rising trend in annual ET for 2003–2016 (0.5 mm/yr) (Table S5 in Supporting Information S1). Therefore, the negative $Trend_{NPI}$ might be the result of increasing ET associated with warming summer air temperatures (Suzuki et al., 2016). The increasing trend of winter discharge and baseflow due to warming temperatures and warming-enhanced permafrost thawing (Hiyama et al., 2023) also contribute to water storage depletion in this basin.

4.2. North America

The Yukon River Basin, located in northwest Canada, experiences severe mass depletion, with $Trend_G$ (-15.4 ± 1.1 mm/yr) significantly lower than $Trend_{LB}$ (-6.9 ± 0.3 mm/yr). The major depletion area is near the Alaska glacial region (Figures S6b and S6d in Supporting Information S1), which may be a result of using $3 \times 3°$ equal-area caps (Wiese et al., 2016). The $Trend_{PI}$ and $Trend_{NPI}$ are 1.2 ± 0.4 and -16.6 ± 1.2 mm/yr, respectively. The NPI mass loss can be attributed to glacier melting, permafrost thaw, and reduced snow cover due to rising temperatures (Long et al., 2017; Rodell et al., 2018; Wang et al., 2015). The glacier mass change rate accounts for 32.6% of the $Trend_G$ (Table S6 in Supporting Information S1). The ongoing decline of glacier mass may continue for a considerable period due to global warming, indicating that the TWS loss appears to be irrecoverable in the Yukon River Basin.

Significant decreasing trends ($Trend_G$: −6.8 ± 0.7 mm/yr; $Trend_{NPI}$: −6.9 ± 0.7 mm/yr) are observed over the middle and eastern regions of the Mackenzie River Basin during 2003–2016 (Figure 3). The mass anomalies in the Mackenzie River Basin show a continuous drop (Figure 7l), similar to the situation in the Yukon River Basin. There may be some irreversibility in the TWS loss in this basin. The shrinking of snow and glaciers has been observed in the Mackenzie River Basin (Zhang et al., 2019). However, glacier melting only contributes a small part to the mass loss (i.e., 8.6%, Table S6 in Supporting Information S1). Additionally, there has been an increasing trend in maximum and minimum temperatures in this basin from 1990 to 2016. The rising temperature trend will lead to increased glacial melting and potentially contribute to increased ET. It should be noted that the estimate of $Trend_G$ in the Mackenzie River Basin has large uncertainty due to possible GIA uncertainty (Figure S7 in Supporting Information S1), which further affects our inferences (Rodell et al., 2018; Scanlon et al., 2018).

Noticeable water gains ($Trend_G$: 6.4 ± 1.4 mm/yr; $Trend_{PI}$: 6.0 ± 0.5 mm/yr) are observed in the Nelson River Basin, exceeding the $Trend_{UB}$ (5.7 ± 0.5 mm/yr). The PI trend can explain 93.8% of the total GRACE trend. The Canadian prairies, located in the hinterland of this basin, contribute to the rise in TWS, which can be attributed to increased precipitation starting in 2004 after a drought period from 2002 to 2004 (Lambert et al., 2013). Two remarkable increases in TWS during 2005–2006 and 2011–2012 can be attributed to abundant precipitation (Figure S5 in Supporting Information S1). The annual precipitation trend is 5.3 mm/yr (2003–2016). Moreover, the annual mean precipitation during 2003–2016 is 502.8 mm/yr, which is 24.5 mm/yr more than the annual average precipitation from 1980 to 2016. Although the PI TWSA can explain the $Trend_G$, the possible uncertainty related to GIA should not be neglected (Figure S7 in Supporting Information S1).

The southwest region of the Continental United States experienced the highest water over-consumption from 2003–2015 (Solander et al., 2017). Combined with drought conditions (Scanlon et al., 2016), extensive groundwater pumping for agricultural irrigation and municipal, industrial, and domestic demands put considerable stress on the Rio Grande Basin (Figure S3 in Supporting Information S1), resulting in a noticeable $Trend_G$ (−6.1 ± 1.1 mm/yr). The $Trend_{NPI}$ accounts for 90.2% of the $Trend_G$, indicating that NPI factors play a dominant role in the TWS depletion of the Rio Grande Basin.

4.3. Africa

In the six large basins of Africa, the $Trend_{PI}$ values are generally small (Table 3), and both $Trend_G$ and $Trend_{NPI}$ are positive, indicating that non-precipitation factors significantly influence the growth of TWS in these basins. However, caution should be exercised due to relatively poor-quality precipitation data and the challenges in reconstructing climate-driven TWS in Africa (Humphrey & Gudmundsson, 2019; Rodell et al., 2018).

The global grid-scale NPI trend map (Figure 3c) shows that the trend of TWS growth in West Africa is more influenced by non-precipitation factors. Significant TWS rise has been recorded in the Niger River Basin during the GRACE period (Scanlon et al., 2016; Werth et al., 2017). $Trend_{NPI}$ (4.7 ± 0.6 mm/yr) accounts for 87.0% of $Trend_G$ (5.4 ± 0.6 mm/yr) in this basin. The PI TWSA can only explain part of the fluctuations of the GRACE TWSA (Figure 7o), which may be a result of uncertainty in the reconstruction. The $Trend_G$, which exceeds the $Trend_{UB}$ (1.6 ± 0.1 mm/yr), can be attributed to the increasing groundwater and land cover changes (Werth et al., 2017).

The Lake Chad Basin ($Trend_G$: 0.9 ± 0.5 mm/yr) experienced a wetting trend during the GRACE period, with increased precipitation reported (Ahmed et al., 2014), particularly during the wettest period from 2012 to 2014 (Ndehedehe et al., 2016). However, due to uncertainties in different precipitation estimates, our study does not show positive precipitation anomalies in 2013 and 2014 (Figure S5p in Supporting Information S1), resulting in no obvious trend in PI TWSA from 2003 to 2016. With the supply of groundwater and tropical water sources, the water level and area of Lake Chad, as observed by altimetry and satellite images, have gradually recovered over the past two decades (Pham-Duc et al., 2020). Furthermore, some areas located in the south of the Lake Chad Basin are highly protected natural resource areas (Mahmood et al., 2019), and agricultural activities are less prevalent in this basin (Buma et al., 2018), contributing to the increase in TWS to a certain extent. However, when compared with $Trend_{UB(M79\text{-}14)}$ (2.9 ± 0.2 mm/yr), the increased $Trend_G$ is no longer significant.

A pronounced TWS increase ($Trend_G$: 4.4 ± 0.8 mm/yr) is observed in the Nile River Basin. However, this trend cannot be explained by precipitation variability ($Trend_{PI}$: 0.1 ± 0.2 mm/yr), and $Trend_{NPI}$ accounts for 97.7% of $Trend_G$. The significant TWS increase is concentrated around Lake Victoria and the upstream area of the Blue

Nile (Figure 3). The possible cause for the observed $Trend_G$ may be the rising regional lake levels, such as Lake Victoria (Hasan et al., 2021; Rodell et al., 2018; Yao et al., 2023). The construction of dams, such as the Grand Ethiopian Renaissance Dam on the Blue Nile River, can also contribute to the rise in the regional water table (Rodell et al., 2018). Due to the scarcity of rain gauges, the $Trend_{PI}$ may be underestimated in the Nile River Basin (Rodell et al., 2018).

In the Jubba River Basin, $Trend_G$ and $Trend_{NPI}$ are calculated as 1.9 ± 0.7 and 2.0 ± 0.7 mm/yr, respectively. The major increase signal is located in the west of this basin (Figure 3), which is likely a result of the rising water levels of nearby lakes, such as Lake Turkana and Abaya (Yao et al., 2023)). Similar to the Lake Chad Basin, the Jubba River Basin also experienced an extreme precipitation event in 2013 (Figure S5r in Supporting Information S1). However, the precipitation factor does not contribute to the long-term increasing trend observed in this basin.

In the Congo River Basin, the decline in precipitation may explain the negative $Trend_{PI}$ (-0.9 ± 0.3 mm/yr). However, despite this, positive trends are observed in $Trend_G$ (2.3 ± 1.2 mm/yr) and $Trend_{NPI}$ (3.2 ± 1.2 mm/yr). The increase in TWS is mainly observed around the upstream area of the Congo River, as well as near Lake Tanganyika and Lake Victoria (Figure 3a). Little is known about the TWSA and the driving factors in the Congo River Basin, despite it being one of the largest basins in the world (Burnett et al., 2020). Previous research has suggested that the Congo River Basin experienced a long-term drying trend from the 1970s to the first 10 years of the 21st century, along with deforestation in the late 20th century, which may have led to rising temperatures and reduced precipitation (Zhou et al., 2014).

The Okavango River Basin is experiencing an apparent wetting trend ($Trend_G$: 10.0 ± 2.0 mm/yr), which exceeds the $Trend_{UB}$ (9.5 ± 0.5 mm/yr) and is also close to $Trend_{UB(M79\text{-}14)}$ (10.1 ± 0.6 mm/yr). A significant increase in TWS is observed in the upstream area of the Okavango River, while no apparent trend is observed in the Okavango Delta (Figure 3a). A significant increase in $Trend_{PI}$ is evident in the middle of this basin, but with a surrounding decline in $Trend_{NPI}$ (Figure 3c), which may result from precipitation uncertainty. The PI TWSA captures the interannual fluctuations of GRACE TWSA (Figure 7t). The precipitation change (70.2 mm/yr) for 2003–2016 relative to 1980–2016 is quite apparent, with the average annual precipitation increasing by 13.8%. An annual precipitation peak in 2006 was also observed in the Okavango River Basin (Figure S5l in Supporting Information S1). Consistent with previous studies, a rapid increase in precipitation from 2006 to 2011 was observed in the Okavango Delta (Rodell et al., 2018). However, the $Trend_{PI}$ (2.1 ± 0.8 mm/yr) appears to underestimate the actual PI trend due to the uncertainty of precipitation estimate, leading to an overestimation of the NPI trend in this basin.

5. Discussion

5.1. The Uncertainties of $Trend_{UB}$ and $Trend_{LB}$ Estimates

Typically, a basin should exhibit equal $Trend_{UB}$ and $Trend_{LB}$ (absolute values) over a long period. However, some basins in our study deviate from this pattern. Among the global 266 basins, there are two large basins, five medium basins, and 12 small basins with an absolute deviation between $Trend_{UB}$ and $Trend_{LB}$ greater than 5 mm/yr. Therefore, the method proposed in this study may perform better in large basins, considering the number of the three basin types.

The quality of input precipitation data is the primary factor influencing the performance of the reconstruction models (Humphrey & Gudmundsson, 2019), which, in turn, affects the estimates of $Trend_{UB/LB}$ in our study. The accuracy of the GRACE-REC/JPL-GSWP3 data set appears to be lower in regions where rainfall gauges and precipitation data are scarce, such as tropical Africa, Central Asia, northern Russia, and South America (M. Chen et al., 2008; Humphrey & Gudmundsson, 2019). As a result, the $Trend_{UB/LB}$ estimates may be underestimated in African basins, and the $Trend_{UB(G79\text{-}14)}$ is significantly smaller than $Trend_{UB(M79\text{-}14)}$ in the Niger River and Lake Chad Basin (Data Set S1). Table 3 presents the small values of $Trend_{UB/LB}$ for African basins, which show considerable discrepancies with the $Trend_{UB/LB}$ estimates from GRACE-REC/JPL-MSWEP. Therefore, caution should be exercised when interpreting the analysis in these regions. Additionally, the reconstructed GSWP3-based GRACE-REC data may be less accurate compared to MSWEP- and ERA5-based data (Humphrey & Gudmundsson, 2019), which can affect our estimates of the upper and lower bounds.

Estimating $Trend_{UB}$, $Trend_{LB}$, and $Trend_{PI}$ in glacial regions (e.g., the Brahmaputra, Indus, and Yukon River Basin) may introduce more uncertainties due to the limitations of the reconstruction method (Deng et al., 2023;

Table 4
The Number of Basins When $Trend_G$ Is Beyond $Trend_{UB/LB}$ Using Different Windows

Window periods	The number of basins with $Trend_G$ is beyond $Trend_{UB/LB}$			
	Large basins	Medium basins	Small basins	Total basins
12 (2004–2015)	14 (13)	26 (22)	42 (41)	82 (76)
12 (2005–2016)	13 (12)	28 (22)	46 (41)	87 (75)
13 (2003–2015)	13 (13)	26 (22)	45 (45)	84 (80)
13 (2004–2016)	14 (13)	28 (23)	50 (47)	92 (83)
14 (2003–2016)	16	27	52	95
15 (2003–2017)	15 (15)	30 (26)	56 (50)	101 (91)
16 (2003–2018)	16 (15)	31 (24)	59 (48)	106 (87)
17 (2003–2019)	17 (13)	35 (24)	67 (47)	119 (84)
18 (2003–2020)	20 (13)	38 (24)	70 (48)	128 (85)
19 (2003–2021)	22 (13)	37 (22)	77 (49)	136 (84)

Note. The parentheses in the first column show the window lengths and corresponding periods for GRACE trend estimates. The parentheses in the second to fifth columns show the numbers of the same basin identified for the corresponding window length and 14-year window.

Humphrey & Gudmundsson, 2019). While the reconstruction model formulation is primarily inspired by the basic principles of hydrological modeling (Humphrey & Gudmundsson, 2019), the reconstructed time series in glacial regions may face additional challenges. This is because glacial regions involve glacier and snow processes, distinct from typical hydrological processes (B. Liu et al., 2022; Yi et al., 2020). Moreover, these regions are often mountainous, and precipitation in these areas tends to be highly variable and of lower quality. Therefore, applying our method to glacial regions requires specialized reconstruction results in the future.

In this study, $Trend_{UB}$ and $Trend_{LB}$ are estimated using one-century GRACE-REC/JPL-GSWP3 data. However, these estimates may be influenced by extreme events. We examined the century-long TWSA time series of 40 large basins worldwide and found that only six basins had $Trend_{UB}$ or $Trend_{LB}$ related to extremes (Figure S8 in Supporting Information S1). It is important to note that these extremes typically occur at the beginning or end of a trend period. While extreme events are only a part of long-term climate-driven TWSA, they demonstrate that basins can experience maximum water loss or gain under natural conditions, which is reasonable to some extent. Furthermore, the impact of short-term extreme events on the 14-year trend estimate is relatively small.

5.2. Impact of Using Different Windows to Evaluate the TWS Trends

The choice of different windows to estimate the trend in TWS is further examined to demonstrate the sensitivity and reliability of this method. We utilized window lengths ranging from 12 to 19 years (Table 4), where the values in parentheses represent the number of the same basins identified using the corresponding window length in this study (i.e., 14-year). Due to a lack of sufficient long GRACE-REC data, $Trend_{PI}$ was not estimated in this comparison. Most basins identified using a 14-year window were also identified using other window lengths. The only basin not identified by the 14-year window, but identified by the 12- and 13-year windows is the Congo River Basin, which exhibits significant interannual variability. Furthermore, the $Trend_{NPI}$ for the period 2003–2016 exceeds the $Trend_{UB}$ in this basin. The 13-year window (i.e., 2003–2015, the third row) is most consistent with the 14-year window, with only four medium-sized basins identified by the 13-year window not included in the 14-year window. We examined these four basins and found that two of them were also identified by $Trend_{NPI}$ (i.e., below the $Trend_{LB}$). Additionally, the 15-year window shows consistency with the 14-year window, followed by the 16-year window.

With the lengthening of the window, more basins are identified using our method (Table 4). This is understandable as the impact of natural variability on the TWS trend would diminish with an extension of time. Consequently, the maximum variation in TWS trends under natural conditions over an extended period would decrease. Similarly, the values of $Trend_{PI}$ would decline over time. While GRACE TWS changes are influenced by a combination of natural variability, climate change, and anthropogenic factors, $Trend_G$ would be more stable than $Trend_{UB/LB}$.

The method presented in this study serves as a valuable tool in the field of GRACE studies, allowing for the assessment of the intensity of GRACE trends on a basin or regional scale over a specific period. It is important to note that as the study period is extended, the estimates of $Trend_{UB/LB}$ and $Trend_{PI}$ for a longer duration may decrease. In cases where a basin exhibits a consistent $Trend_G$ or $Trend_{PI}$, it becomes easier to identify and highlight the irreversibility of such trends.

6. Conclusions

Here we proposed a novel criterion to interpret the trends and drivers (precipitation-induced, and non-precipitation-induced) in GRACE by comparing the GRACE water storage trends with the trend bounds under natural climate variability determined by century-long GRACE-REC data set. Our results reveal that the trends ($Trend_G$, $Trend_{PI}$, or $Trend_{NPI}$) in 115 basins (20 large, 34 medium, 61 small) exceed the bound values ($Trend_{UB/LB}$). Furthermore, over 70% of global basins exhibit an absolute deviation between $Trend_{UB(M79-14)}$ and

$Trend_{UB(G79\text{-}14)}$, as well as between $Trend_{UB(M79\text{-}14)}$ and $Trend_{UB(G79\text{-}14)}$, of less than 2 mm/yr, indicating the reliability of the $Trend_{UB}$ and $Trend_{LB}$ estimates to some extent.

The method proposed in this study enhances the interpretation and assessment of TWS trends in specific basins and facilitates the analysis of potential drivers through the estimates of $Trend_G$, $Trend_{PI}$, and $Trend_{NPI}$. In basins where only $Trend_G$ exceeds the bound values (e.g., the Yangtze River Basin), it is more likely that TWS will return to normal levels. In basins where both $Trend_G$ and $Trend_{PI}$ surpass $Trend_{UB}$, precipitation plays a significant role in TWS variations, as observed in the Nelson River Basin. On the other hand, when both $Trend_G$ and $Trend_{NPI}$ are lower than $Trend_{LB}$, TWS deficits are primarily attributable to factors such as glacier melting (e.g., the Yukon, Mackenzie, and Chubut River Basin) and groundwater withdrawal (e.g., the Yongding River [North China], Ganges, Kura, Shatt Al Arab, Brazos, and Colorado (Texas) Basins).

While GRACE observations provide valuable insights into the natural variability of TWS, $Trend_G$ alone may not present a comprehensive picture of TWS increases or losses given the relatively short time span of GRACE observations. The method proposed in this study serves as a criterion for reassessing the severity of TWS deficits during the GRACE period, contributing to the sustainable development and management of water resources.

Conflict of Interest

The authors declare no conflicts of interest relevant to this study.

Data Availability Statement

GRACE data can be publicly obtained from Wiese et al. (2019). ICE-5G (VM2) data can be publicly obtained from Peltier (2004). ICE-6G_D (VM5a) data can be publicly obtained from Purcell et al. (2016). GRACE-REC data set can be publicly obtained from Humphrey and Gudmundsson (2019). The boundary of global basins can be publicly obtained from Global Runoff Data Centre (GRDC, 2020). Precipitation data can be publicly obtained from Beck et al. (2019). Evapotranspiration data can be publicly obtained from Martens et al. (2017). Global Map of Irrigation Areas can be publicly obtained from Siebert et al. (2013). Water use data can be publicly obtained from Gosling et al. (2023). Glacier outline data can be publicly obtained from Consortium (2017). Glacier mass loss data can be publicly obtained from Hugonnet et al. (2021). Maps and figures were created by Generic Mapping Tools (GMT) version 6 (Wessel et al., 2019), available at https://www.generic-mapping-tools.org/download/. The presented data set (i.e., Data Set S1 and S2, (Zhong, Tian, et al., 2023)) can be publicly downloaded from https://doi.org/10.6084/m9.figshare.24452380.

Acknowledgments

This work was funded jointly by the Natural Science Foundation of China (Grants 42061134010, 42004073, 42374032, 42274111, and 41874095), Open Fund of State Key Laboratory of Remote Sensing Science (Grant OFSLRSS202107), and Fundamental Research Funds for the Central Universities, China University of Geosciences (Wuhan) (26420190050-CUGL190805). B. D. Vishwakarma is supported by the IISc-ISRO STC Grant (SP/ISTC-22-0004). W. Feng is also supported by the Natural Science Fund for Distinguished Young Scholars of Hubei Province, China (Grant 2019CFA091).

References

Ahmed, M., Sultan, M., Wahr, J., & Yan, E. (2014). The use of GRACE data to monitor natural and anthropogenic induced variations in water availability across Africa. *Earth-Science Reviews*, *136*, 289–300. https://doi.org/10.1016/j.earscirev.2014.05.009

Amiri, V., Ali, S., & Sohrabi, N. (2023). Estimating the spatio-temporal assessment of GRACE/GRACE-FO derived groundwater storage depletion and validation with in-situ water quality data (Yazd province, central Iran). *Journal of Hydrology*, *620*, 129416. https://doi.org/10.1016/j.jhydrol.2023.129416

An, L., Wang, J., Huang, J., Pokhrel, Y., Hugonnet, R., Wada, Y., et al. (2021). Divergent causes of terrestrial water storage decline between drylands and humid regions globally. *Geophysical Research Letters*, *48*(23), e2021GL095035. https://doi.org/10.1029/2021gl095035

Bai, H., Ming, Z., Zhong, Y., Zhong, M., Kong, D., & Ji, B. (2022). Evaluation of evapotranspiration for exorheic basins in China using an improved estimate of terrestrial water storage change. *Journal of Hydrology*, *610*, 127885. https://doi.org/10.1016/j.jhydrol.2022.127885

Beck, H. E., Wood, E. F., Pan, M., Fisher, C. K., Miralles, D. G., van Dijk, A. I. J. M., et al. (2019). MSWEP V2 global 3-hourly 0.1° precipitation: Methodology and quantitative assessment. *Bulletin of the American Meteorological Society*, *100*(3), 473–500. https://doi.org/10.1175/bams-d-17-0138.1

Boergens, E., Güntner, A., Dobslaw, H., & Dahle, C. (2020). Quantifying the central European droughts in 2018 and 2019 with GRACE follow-on. *Geophysical Research Letters*, *47*(14), e2020GL087285. https://doi.org/10.1029/2020gl087285

Buma, W. G., Lee, S. I., & Seo, J. Y. (2018). Recent surface water extent of Lake Chad from multispectral sensors and GRACE. *Sensors*, *18*(7), 2082. https://doi.org/10.3390/s18072082

Burnett, M. W., Quetin, G. R., & Konings, A. G. (2020). Data-driven estimates of evapotranspiration and its controls in the Congo Basin. *Hydrology and Earth System Sciences*, *24*(8), 4189–4211. https://doi.org/10.5194/hess-24-4189-2020

Chao, N., Jin, T., Cai, Z., Chen, G., Liu, X., Wang, Z., & Yeh, P. J. (2021). Estimation of component contributions to total terrestrial water storage change in the Yangtze river basin. *Journal of Hydrology*, *595*, 125661. https://doi.org/10.1016/j.jhydrol.2020.125661

Chao, N., Luo, Z., Wang, Z., & Jin, T. (2018). Retrieving groundwater depletion and drought in the Tigris-euphrates basin between 2003 and 2015. *Groundwater*, *56*(5), 770–782. https://doi.org/10.1111/gwat.12611

Chen, J., Famiglietti, J. S., Scanlon, B. R., & Rodell, M. (2016). Groundwater storage changes: Present status from GRACE observations. *Surveys in Geophysics*, *37*(2), 397–417. https://doi.org/10.1007/s10712-015-9332-4

Chen, J., Wilson, C. R., Tapley, B. D., Blankenship, D. D., & Ivins, E. R. (2007). Patagonia icefield melting observed by gravity recovery and climate experiment (GRACE). *Geophysical Research Letters*, *34*(22), L22501. https://doi.org/10.1029/2007GL031871

Chen, M., Shi, W., Xie, P., Silva, V. B., Kousky, V. E., Wayne Higgins, R., & Janowiak, J. E. (2008). Assessing objective techniques for gauge-based analyses of global daily precipitation. *Journal of Geophysical Research*, *113*(D4), D04110. https://doi.org/10.1029/2007JD009132

Chen, X., Long, D., Hong, Y., Zeng, C., & Yan, D. (2017). Improved modeling of snow and glacier melting by a progressive two-stage calibration strategy with GRACE and multisource data: How snow and glacier meltwater contributes to the runoff of the Upper Brahmaputra River basin? *Water Resources Research*, *53*(3), 2431–2466. https://doi.org/10.1002/2016wr019656

Consortium, R. (2017). A dataset of global glacier outlines: Version 6.0 [Dataset]. NSIDC: National Snow and Ice Data Center. https://doi.org/10.7265/N5-RGI-60

Davybida, L., & Kuzmenko, E. (2018). Assessment of observation network and state of exploration as to groundwater dynamics within Ukrainian hydrogeological province of Dnieper River. *Geomatics and Environmental Engineering*, *12*(2), 19. https://doi.org/10.7494/geom.2018.12.2.19

Deng, S., Liu, Y., & Zhang, W. (2023). A comprehensive evaluation of GRACE-like terrestrial water storage (TWS) reconstruction products at an interannual scale during 1981–2019. *Water Resources Research*, *59*(3), e2022WR034381. https://doi.org/10.1029/2022wr034381

Famiglietti, J. S. (2014). The global groundwater crisis. *Nature Climate Change*, *4*(11), 945–948. https://doi.org/10.1038/nclimate2425

Famiglietti, J. S., Cazenave, A., Eicker, A., Reager, J., Rodell, M., & Velicogna, I. (2015). Satellites provide the big picture. *Science*, *349*(6249), 684–685. https://doi.org/10.1126/science.aac9238

Feng, W., Zhong, M., Lemoine, J.-M., Biancale, R., Hsu, H.-T., & Xia, J. (2013). Evaluation of groundwater depletion in North China using the Gravity Recovery and Climate Experiment (GRACE) data and ground-based measurements. *Water Resources Research*, *49*(4), 2110–2118. https://doi.org/10.1002/wrcr.20192

Gleeson, T., Wada, Y., Bierkens, M. F., & van Beek, L. P. (2012). Water balance of global aquifers revealed by groundwater footprint. *Nature*, *488*(7410), 197–200. https://doi.org/10.1038/nature11295

Gosling, S. N., Schmied, H. M., Burek, P., Chang, J., Ciais, P., Döll, P., et al. (2023). ISIMIP2b simulation data from the global water sector (v1.0) [Dataset]. ISIMIP Repository. https://doi.org/10.48364/ISIMIP.626689

GRDC. (2020). WMO basins and sub-basins/global runoff data Centre, GRDC [Dataset]. 3rd, rev. ext. ed. Federal Institute of Hydrology (BfG). Retrieved from https://www.bafg.de/SharedDocs/ExterneLinks/GRDC/mrb_shp_zip.html

Hasan, E., Tarhule, A., & Kirstetter, P.-E. (2021). Twentieth and twenty-first century water storage changes in the Nile River Basin from GRACE/GRACE-FO and modeling. *Remote Sensing*, *13*(5), 953. https://doi.org/10.3390/rs13050953

Hiyama, T., Park, H., Kobayashi, K., Lebedeva, L., & Gustafsson, D. (2023). Contribution of summer net precipitation to winter river discharge in permafrost zone of the Lena River basin. *Journal of Hydrology*, *616*, 128797. https://doi.org/10.1016/j.jhydrol.2022.128797

Huang, Z., Pan, Y., Gong, H., Yeh, P. J. F., Li, X., Zhou, D., & Zhao, W. (2015). Subregional-scale groundwater depletion detected by GRACE for both shallow and deep aquifers in North China Plain. *Geophysical Research Letters*, *42*(6), 1791–1799. https://doi.org/10.1002/2014gl062498

Huggins, X., Gleeson, T., Kummu, M., Zipper, S. C., Wada, Y., Troy, T. J., & Famiglietti, J. S. (2022). Hotspots for social and ecological impacts from freshwater stress and storage loss. *Nature Communications*, *13*(1), 439. https://doi.org/10.1038/s41467-022-28029-w

Hugonnet, R., McNabb, R., Berthier, E., Menounos, B., Nuth, C., Girod, L., et al. (2021). Accelerated global glacier mass loss in the early twenty-first century. *Nature*, *592*(7856), 726–731. https://doi.org/10.1038/s41586-021-03436-z

Humphrey, V., & Gudmundsson, L. (2019). GRACE-REC: A reconstruction of climate-driven water storage changes over the last century. *Earth System Science Data*, *11*(3), 1153–1170. https://doi.org/10.5194/essd-11-1153-2019

Humphrey, V., Rodell, M., & Eicker, A. (2023). Using satellite-based terrestrial water storage data: A review. *Surveys in Geophysics*, *44*(5), 1489–1517. https://doi.org/10.1007/s10712-022-09754-9

Joodaki, G., Wahr, J., & Swenson, S. (2014). Estimating the human contribution to groundwater depletion in the Middle East, from GRACE data, land surface models, and well observations. *Water Resources Research*, *50*(3), 2679–2692. https://doi.org/10.1002/2013wr014633

Kundzewicz, Z. W., Mata, L. J., Arnell, N., Doll, P., Kabat, P., Jimenez, B., et al. (2007). Freshwater resources and their management. In *Climate change 2007: Impacts, Adaptation and vulnerability—contribution of working group II to the fourth assessment report of the intergovernmental panel on climate change* (pp. 173–210). Retrieved from http://www.ipcc.ch/pdf/assessment-report/ar4/wg2/ar4-wg2-chapter3.pdf

Lambert, A., Huang, J., van der Kamp, G., Henton, J., Mazzotti, S., James, T. S., et al. (2013). Measuring water accumulation rates using GRACE data in areas experiencing glacial isostatic adjustment: The Nelson River basin. *Geophysical Research Letters*, *40*(23), 6118–6122. https://doi.org/10.1002/2013gl057973

Landerer, F. W., Flechtner, F. M., Save, H., Webb, F. H., Bandikova, T., Bertiger, W. I., et al. (2020). Extending the global mass change data record: GRACE follow-on instrument and science data performance. *Geophysical Research Letters*, *47*(12), e2020GL088306. https://doi.org/10.1029/2020GL088306

Li, X., Long, D., Scanlon, B. R., Mann, M. E., Li, X., Tian, F., et al. (2022). Climate change threatens terrestrial water storage over the Tibetan Plateau. *Nature Climate Change*, *12*(9), 801–807. https://doi.org/10.1038/s41558-022-01443-0

Liu, B., Zou, X., Yi, S., Sneeuw, N., Li, J., & Cai, J. (2022). Reconstructing GRACE-like time series of high mountain glacier mass anomalies. *Remote Sensing of Environment*, *280*, 113177. https://doi.org/10.1016/j.rse.2022.113177

Liu, P. W., Famiglietti, J. S., Purdy, A. J., Adams, K. H., McEvoy, A. L., Reager, J. T., et al. (2022). Groundwater depletion in California's Central Valley accelerates during megadrought. *Nature Communications*, *13*(1), 7825. https://doi.org/10.1038/s41467-022-35582-x

Long, D., Pan, Y., Zhou, J., Chen, Y., Hou, X., Hong, Y., et al. (2017). Global analysis of spatiotemporal variability in merged total water storage changes using multiple GRACE products and global hydrological models. *Remote Sensing of Environment*, *192*, 198–216. https://doi.org/10.1016/j.rse.2017.02.011

Long, D., Yang, W., Scanlon, B. R., Zhao, J., Liu, D., Burek, P., et al. (2020). South-to-North Water Diversion stabilizing Beijing's groundwater levels. *Nature Communications*, *11*(1), 1–10. https://doi.org/10.1038/s41467-020-17428-6

Long, D., Yang, W., Sun, Z., Cui, Y., Zhang, C., & Cui, Y. (2023). GRACE satellite-based estimation of groundwater storage changes and water balance analysis for the Haihe River Basin. *Journal of Hydraulic Engineering*, *54*(03), 255–267. https://doi.org/10.13243/j.cnki.slxb.20220743

Luthcke, S. B., Sabaka, T., Loomis, B., Arendt, A., McCarthy, J., & Camp, J. (2013). Antarctica, Greenland and Gulf of Alaska land-ice evolution from an iterated GRACE global mascon solution. *Journal of Glaciology*, *59*(216), 613–631. https://doi.org/10.3189/2013JoG12J147

Mahmood, R., Jia, S., & Zhu, W. (2019). Analysis of climate variability, trends, and prediction in the most active parts of the Lake Chad basin, Africa. *Scientific Reports*, *9*(1), 6317. https://doi.org/10.1038/s41598-019-42811-9

Martens, B., Miralles, D. G., Lievens, H., van der Schalie, R., de Jeu, R. A. M., Fernández-Prieto, D., et al. (2017). GLEAM v3: Satellite-based land evaporation and root-zone soil moisture. *Geoscientific Model Development*, *10*(5), 1903–1925. https://doi.org/10.5194/gmd-10-1903-2017

Mekonnen, M. M., & Hoekstra, A. Y. (2016). Four billion people facing severe water scarcity. *Science Advances*, *2*(2), e1500323. https://doi.org/10.1126/sciadv.1500323

Mo, X., Wu, J., Wang, Q., & Zhou, H. (2016). Variations in water storage in China over recent decades from GRACE observations and GLDAS. *Natural Hazards and Earth System Sciences*, *16*(2), 469–482. https://doi.org/10.5194/nhess-16-469-2016

Ndehedehe, C. E., Agutu, N. O., Okwuashi, O., & Ferreira, V. G. (2016). Spatio-temporal variability of droughts and terrestrial water storage over Lake Chad Basin using independent component analysis. *Journal of Hydrology*, *540*, 106–128. https://doi.org/10.1016/j.jhydrol.2016.05.068

Peltier, W. R. (2004). Global glacial isostasy and the surface of the ice-age Earth: The ICE-5G (VM2) model and GRACE. *Annual Review of Earth and Planetary Sciences*, *32*(1), 111–149. https://doi.org/10.1146/annurev.earth.32.082503.144359

Pham-Duc, B., Sylvestre, F., Papa, F., Frappart, F., Bouchez, C., & Cretaux, J. F. (2020). The Lake Chad hydrology under current climate change. *Scientific Reports*, *10*(1), 5498. https://doi.org/10.1038/s41598-020-62417-w

Pichura, V., Potravka, L., Skrypchuk, P., & Stratichuk, N. (2020). Anthropogenic and climatic causality of changes in the hydrological regime of the Dnieper River. *Journal of Ecological Engineering*, *21*(4), 1–10. https://doi.org/10.12911/22998993/119521

Pokhrel, Y., Felfelani, F., Satoh, Y., Boulange, J., Burek, P., Gadeke, A., et al. (2021). Global terrestrial water storage and drought severity under climate change. *Nature Climate Change*, *11*(3), 226–233. https://doi.org/10.1038/s41558-020-00972-w

Purcell, A., Tregoning, P., & Dehecq, A. (2016). An assessment of the ICE6G_C(VM5a) glacial isostatic adjustment model. *Journal of Geophysical Research: Solid Earth*, *121*(5), 3939–3950. https://doi.org/10.1002/2015jb012742

Ramillien, G., Famiglietti, J. S., & Wahr, J. (2008). Detection of continental hydrology and glaciology signals from GRACE: A review. *Surveys in Geophysics*, *29*(4–5), 361–374. https://doi.org/10.1007/s10712-008-9048-9

Ran, J., Ditmar, P., Liu, L., Xiao, Y., Klees, R., & Tang, X. Y. (2021). Analysis and mitigation of biases in Greenland ice sheet mass balance trend estimates from GRACE mascon products. *Journal of Geophysical Research: Solid Earth*, *126*(7), e2020JB020880. https://doi.org/10.1029/2020JB020880

Ran, Y., Zhong, M., Chen, W., Zhong, Y., & Feng, W. (2021). Monitoring the extreme drought in the middle and lower reaches of the Yangtze River in 2019 from GRACE-FO satellites. *Chinese Science Bulletin*, *66*(1), 107–117. https://doi.org/10.1360/tb-2020-0375

Richey, A. S., Thomas, B. F., Lo, M. H., Reager, J. T., Famiglietti, J. S., Voss, K., et al. (2015). Quantifying renewable groundwater stress with GRACE. *Water Resources Research*, *51*(7), 5217–5238. https://doi.org/10.1002/2015WR017349

Rodell, M., Famiglietti, J. S., Wiese, D. N., Reager, J. T., Beaudoing, H. K., Landerer, F. W., & Lo, M. H. (2018). Emerging trends in global freshwater availability. *Nature*, *557*(7707), 651–659. https://doi.org/10.1038/s41586-018-0123-1

Rodell, M., & Li, B. (2023). Changing intensity of hydroclimatic extreme events revealed by GRACE and GRACE-FO. *Nature Water*, *1*(3), 241–248. https://doi.org/10.1038/s44221-023-00040-5

Scanlon, B. R., Fakhreddine, S., Rateb, A., de Graaf, I., Famiglietti, J., Gleeson, T., et al. (2023). Global water resources and the role of groundwater in a resilient water future. *Nature Reviews Earth & Environment*, *4*(2), 87–101. https://doi.org/10.1038/s43017-022-00378-6

Scanlon, B. R., Rateb, A., Anyamba, A., Kebede, S., MacDonald, A. M., Shamsudduha, M., et al. (2022). Linkages between GRACE water storage, hydrologic extremes, and climate teleconnections in major African aquifers. *Environmental Research Letters*, *17*(1), 014046. https://doi.org/10.1088/1748-9326/ac3bfc

Scanlon, B. R., Zhang, Z., Save, H., Sun, A. Y., Muller Schmied, H., van Beek, L. P. H., et al. (2018). Global models underestimate large decadal declining and rising water storage trends relative to GRACE satellite data. *Proceedings of the National Academy of Sciences of the United States of America*, *115*(6), E1080–E1089. https://doi.org/10.1073/pnas.1704665115

Scanlon, B. R., Zhang, Z., Save, H., Wiese, D. N., Landerer, F. W., Long, D., et al. (2016). Global evaluation of new GRACE mascon products for hydrologic applications. *Water Resources Research*, *52*(12), 9412–9429. https://doi.org/10.1002/2016wr019494

Shamsudduha, M., & Taylor, R. G. (2020). Groundwater storage dynamics in the world's large aquifer systems from GRACE: Uncertainty and role of extreme precipitation. *Earth System Dynamics*, *11*(3), 755–774. https://doi.org/10.5194/esd-11-755-2020

Shen, Z., Zhang, Q., Singh, V. P., Pokhrel, Y., Li, J., Xu, C. Y., & Wu, W. (2022). Drying in the low-latitude Atlantic Ocean contributed to terrestrial water storage depletion across Eurasia. *Nature Communications*, *13*(1), 1849. https://doi.org/10.1038/s41467-022-29544-6

Shi, W., Wang, M., & Guo, W. (2014). Long-term hydrological changes of the Aral Sea observed by satellites. *Journal of Geophysical Research: Oceans*, *119*(6), 3313–3326. https://doi.org/10.1002/2014jc009988

Siebert, S., Henrich, V., Frenken, K., & Burke, J. (2013). Update of the digital global map of irrigation areas (GMIA) to version 5 [Dataset]. Rheinische Friedrich-Wilhelms-University, Food and Agriculture Organization of the United Nations. https://doi.org/10.13140/2.1.2660.6728

Solander, K. C., Reager, J. T., Wada, Y., Famiglietti, J. S., & Middleton, R. S. (2017). GRACE satellite observations reveal the severity of recent water over-consumption in the United States. *Scientific Reports*, *7*(1), 8723. https://doi.org/10.1038/s41598-017-07450-y

Suzuki, K., Matsuo, K., & Hiyama, T. (2016). Satellite gravimetry-based analysis of terrestrial water storage and its relationship with run-off from the Lena River in eastern Siberia. *International Journal of Remote Sensing*, *37*(10), 2198–2210. https://doi.org/10.1080/01431161.2016.1165890

Suzuki, K., Park, H., Makarieva, O., Kanamori, H., Hori, M., Matsuo, K., et al. (2021). Effect of permafrost thawing on discharge of the Kolyma River, northeastern Siberia. *Remote Sensing*, *13*(21), 4389. https://doi.org/10.3390/rs13214389

Syed, T. H., Famiglietti, J. S., Chambers, D. P., Willis, J. K., & Hilburn, K. (2010). Satellite-based global-ocean mass balance estimates of interannual variability and emerging trends in continental freshwater discharge. *Proceedings of the National Academy of Sciences of the United States of America*, *107*(42), 17916–17921. https://doi.org/10.1073/pnas.1003292107

Tabari, H., Hosseinzadehtalaei, P., Thiery, W., & Willems, P. (2021). Amplified drought and flood risk under future socioeconomic and climatic change. *Earth's Future*, *9*(10), e2021EF002295. https://doi.org/10.1029/2021ef002295

Tapley, B. D., Bettadpur, S., Watkins, M., & Reigber, C. (2004). The gravity recovery and climate experiment: Mission overview and early results. *Geophysical Research Letters*, *31*(9), L09607. https://doi.org/10.1029/2004gl019920

Tapley, B. D., Watkins, M. M., Flechtner, F., Reigber, C., Bettadpur, S., Rodell, M., et al. (2019). Contributions of GRACE to understanding climate change. *Nature Climate Change*, *5*(5), 358–369. https://doi.org/10.1038/s41558-019-0456-2

Taylor, R. G., Scanlon, B., Döll, P., Rodell, M., van Beek, R., Wada, Y., et al. (2013). Ground water and climate change. *Nature Climate Change*, *3*(4), 322–329. https://doi.org/10.1038/nclimate1744

Tiwari, V. M., Wahr, J., & Swenson, S. (2009). Dwindling groundwater resources in northern India, from satellite gravity observations. *Geophysical Research Letters*, *36*(18), L18401. https://doi.org/10.1029/2009gl039401

Turner, S. W. D., Hejazi, M., Calvin, K., Kyle, P., & Kim, S. (2019). A pathway of global food supply adaptation in a world with increasingly constrained groundwater. *Science of the Total Environment*, *673*, 165–176. https://doi.org/10.1016/j.scitotenv.2019.04.070

Velicogna, I., Mohajerani, Y., Landerer, F., Mouginot, J., Noel, B., Rignot, E., et al. (2020). Continuity of ice sheet mass loss in Greenland and Antarctica from the GRACE and GRACE follow-on missions. *Geophysical Research Letters*, *47*(8), e2020GL087291. https://doi.org/10.1029/2020gl087291

Vishwakarma, B. D., Bates, P., Sneeuw, N., Westaway, R. M., & Bamber, J. L. (2021). Re-assessing global water storage trends from GRACE time series. *Environmental Research Letters*, *16*(3), 034005. https://doi.org/10.1088/1748-9326/abd4a9

Vishwakarma, B. D., Devaraju, B., & Sneeuw, N. (2016). Minimizing the effects of filtering on catchment scale GRACE solutions. *Water Resources Research*, *52*(8), 5868–5890. https://doi.org/10.1002/2016wr018960

Vorosmarty, C. J., McIntyre, P. B., Gessner, M. O., Dudgeon, D., Prusevich, A., Green, P., et al. (2010). Global threats to human water security and river biodiversity. *Nature*, *467*(7315), 555–561. https://doi.org/10.1038/nature09440

Voss, K. A., Famiglietti, J. S., Lo, M., Linage, C., Rodell, M., & Swenson, S. C. (2013). Groundwater depletion in the Middle East from GRACE with implications for transboundary water management in the Tigris-Euphrates-Western Iran region. *Water Resources Research*, *49*(2), 904–914. https://doi.org/10.1002/wrcr.20078

Wang, S., Huang, J., Yang, D., Pavlic, G., & Li, J. (2015). Long-term water budget imbalances and error sources for cold region drainage basins. *Hydrological Processes*, *29*(9), 2125–2136. https://doi.org/10.1002/hyp.10343

Watkins, M. M., Wiese, D. N., Yuan, D. N., Boening, C., & Landerer, F. W. (2015). Improved methods for observing Earth's time variable mass distribution with GRACE using spherical cap mascons. *Journal of Geophysical Research: Solid Earth*, *120*(4), 2648–2671. https://doi.org/10.1002/2014JB011547

Werth, S., White, D., & Bliss, D. W. (2017). GRACE detected rise of groundwater in the Sahelian Niger River Basin. *Journal of Geophysical Research: Solid Earth*, *122*(12), 10459–10477. https://doi.org/10.1002/2017jb014845

Wessel, P., Luis, J. F., Uieda, L., Scharroo, R., Wobbe, F., Smith, W. H. F., & Tian, D. (2019). The generic mapping tools version 6. *Geochemistry, Geophysics, Geosystems*, *20*(11), 5556–5564. https://doi.org/10.1029/2019GC008515

Wiese, D., Landerer, F. W., & Watkins, M. M. (2016). Quantifying and reducing leakage errors in the JPL RL05M GRACE mascon solution. *Water Resources Research*, *52*(9), 7490–7502. https://doi.org/10.1002/2016wr019344

Wiese, D., Yuan, D., Boening, C., Landerer, F. W., & Watkins, M. (2019). JPL GRACE and GRACE-FO mascon ocean, ice, and hydrology equivalent water height coastal resolution improvement (CRI) filtered release 06 version 02 [Dataset]. PO.DAAC. https://doi.org/10.5067/TEMSC-3JC62

Wouters, B., Bonin, J. A., Chambers, D. P., Riva, R. E., Sasgen, I., & Wahr, J. (2014). GRACE, time-varying gravity, Earth system dynamics and climate change. *Reports on Progress in Physics*, *77*(11), 116801. https://doi.org/10.1088/0034-4885/77/11/116801

Xie, J., Xu, Y., Wang, Y., Gu, H., Wang, F., & Pan, S. (2019). Influences of climatic variability and human activities on terrestrial water storage variations across the Yellow River basin in the recent decade. *Journal of Hydrology*, *579*, 124218. https://doi.org/10.1016/j.jhydrol.2019.124218

Yao, F., Livneh, B., Rajagopalan, B., Wang, J., Crétaux, J.-F., Wada, Y., & Berge-Nguyen, M. (2023). Satellites reveal widespread decline in global lake. *Science*, *380*(6646), 743–749. https://doi.org/10.1126/science.abo2812

Yi, S., Song, C., Heki, K., Kang, S., Wang, Q., & Chang, L. (2020). Satellite-observed monthly glacier and snow mass changes in southeast Tibet: Implication for substantial meltwater contribution to the Brahmaputra. *The Cryosphere*, *14*(7), 2267–2281. https://doi.org/10.5194/tc-14-2267-2020

Zhang, Y., He, B., Guo, L., Liu, J., & Xie, X. (2019). The relative contributions of precipitation, evapotranspiration, and runoff to terrestrial water storage changes across 168 river basins. *Journal of Hydrology*, *579*, 124194. https://doi.org/10.1016/j.jhydrol.2019.124194

Zhao, F., Long, D., Li, X., Huang, Q., & Han, P. (2022). Rapid glacier mass loss in the Southeastern Tibetan Plateau since the year 2000 from satellite observations. *Remote Sensing of Environment*, *270*, 112853. https://doi.org/10.1016/j.rse.2021.112853

Zhong, Y., Bai, H., Feng, W., Lu, J., & Humphrey, V. (2023). Separating the precipitation- and non-precipitation- driven water storage trends in China. *Water Resources Research*, *59*(3), e2022WR033261. https://doi.org/10.1029/2022wr033261

Zhong, Y., Tian, B., Vishwakarma, B. D., Feng, W., Wu, Y., Bai, H., et al. (2023). Trend estimation: Trend bound ($Trend_{UB/LB}$), GRACE trend ($Trend_{G}$), PI trend ($trend_{PI}$), and NPI trend ($Trend_{NPI}$) [Dataset]. figshare. https://doi.org/10.6084/m9.figshare.24452380

Zhou, L., Tian, Y., Myneni, R. B., Ciais, P., Saatchi, S., Liu, Y. Y., et al. (2014). Widespread decline of Congo rainforest greenness in the past decade. *Nature*, *509*(7498), 86–90. https://doi.org/10.1038/nature13265

Zhu, Y., Liu, S., Yi, Y., Xie, F., Grunwald, R., Miao, W., et al. (2021). Overview of terrestrial water storage changes over the Indus River Basin based on GRACE/GRACE-FO solutions. *Science of the Total Environment*, *799*, 149366. https://doi.org/10.1016/j.scitotenv.2021.149366